AIMS Energy, 12(1): 321–349.
DOI: 10.3934/energy.2024016
Received: 23 November 2023
Revised: 10 January 2024
Accepted: 23 January 2024
Published: 05 February 2024

http://www.aimspress.com/journal/energy

Research article

A novel binary genetic differential evolution optimization algorithm for wind layout problems

Yanting Liu[1], Zhe Xu[2,*], Yongjia Yu[1] and Xingzhi Chang[1]

[1] Changzhou College of Information Technology, Changzhou, 213032 China
[2] School of Computer Information & Engineering, Changzhou Institute of Technology, Changzhou, 213032 China

* **Correspondence:** Email: xuz@czust.edu.cn; Tel: +8651988517725.

Abstract: This paper addresses the increasingly critical issue of environmental optimization in the context of rapid economic development, with a focus on wind farm layout optimization. As the demand for sustainable resource management, climate change mitigation, and biodiversity conservation rises, so does the complexity of managing environmental impacts and promoting sustainable practices. Wind farm layout optimization, a vital subset of environmental optimization, involves the strategic placement of wind turbines to maximize energy production and minimize environmental impacts. Traditional methods, such as heuristic approaches, gradient-based optimization, and rule-based strategies, have been employed to tackle these challenges. However, they often face limitations in exploring the solution space efficiently and avoiding local optima. To advance the field, this study introduces LSHADE-SPAGA, a novel algorithm that combines a binary genetic operator with the LSHADE differential evolution algorithm, effectively balancing global exploration and local exploitation capabilities. This hybrid approach is designed to navigate the complexities of wind farm layout optimization, considering factors like wind patterns, terrain, and land use constraints. Extensive testing, including 156 instances across different wind scenarios and layout constraints, demonstrates LSHADE-SPAGA's superiority over seven state-of-the-art algorithms in both the ability of jumping out of the local optima and solution quality.

Keywords: sustainable resource management; energy optimization problems; wind farm layout; genetic algorithms; differential evolution

1. Introduction

With rapid economic development, the issue of environmental optimization is becoming increasingly important [1, 2]. Resolving environmental optimization problems is essential for

achieving a harmonious balance between human activities and the natural environment [3, 4]. It is crucial for several reasons, including sustainable resource management, climate change mitigation and adaptation, economic and social stability, and biodiversity conservation, etc [5]. However, these problems are very challenging in the context of managing and preserving natural resources, minimizing environmental impact, and promoting sustainable practices. They involve finding the best possible solutions to complex issues related to environmental management and conservation. The overarching goal is to balance human activities with the need to protect and sustain the environment for current and future generations [6].

Wind layout optimization problems [7] are a subset of environmental optimization problems that focus on the efficient placement of wind turbines within a designated area to maximize energy production and economic viability while minimizing environmental impact [8]. The goal is to find the optimal arrangement of wind turbines to harness wind energy effectively, considering factors such as wind patterns, terrain, and land use constraints [9]. Wind farm layout optimization poses challenges due to site-specific factors, such as varying wind patterns and terrain, creating uncertainties in modeling and forecasting. Balancing conflicting objectives, like maximizing energy output while minimizing wake effects, adds complexity. This process requires a multidisciplinary approach, integrating expertise from engineering, meteorology, economics, and environmental science, while navigating regulatory, stakeholder, and data limitations [10, 11]. Despite these challenges, optimizing layouts is crucial for enhancing wind energy efficiency and requires advanced computational methods and constant adaptation to technological advancements [12–15].

Various methods have been proposed for wind farm layout optimization, which typically involve heuristic approaches and iterative design processes based on expert knowledge and simulation techniques [16–22]. Greedy algorithms make sequential decisions based on locally optimal choices, and a greedy approach might involve placing turbines one by one, considering immediate benefits without considering the overall long-term optimal solution [23]. Gradient-based optimization methods involve iteratively adjusting the layout parameters based on the gradient of an objective function (like power output) to reach a local optimum. However, they can get trapped in local optima and might not find the global best solution [24]. Rule-based approaches involve applying predefined rules or guidelines based on expert knowledge and empirical data, for instance, considering wind direction, turbine spacing, and wake effects to manually design layouts [25]. Inspired by natural selection, genetic algorithms involve generating a population of potential solutions (layouts), combining and mutating them iteratively to evolve towards an optimal or near-optimal solution for the wind farm layout [26]. These methods rely on expert knowledge, iterative processes, and simulations to design layouts by considering factors like turbine placement, wind direction, and wake effects. Meta-heuristic algorithms, [27–33] like simulated annealing, particle swarm optimization, or ant colony optimization, involve exploring the search space efficiently, often by mimicking behaviors found in nature, to find an optimal layout considering various constraints and objectives [34–36]. They often require substantial computational resources, may get stuck in local optima, and might not capture the full complexity of wind behavior [37]. Recent advancements in computational capabilities and machine learning have led to more sophisticated, data-driven optimization techniques that aim for more accurate and efficient wind farm layouts by integrating traditional methods with advanced modeling and learning algorithms [38–40].

Among the aforementioned methods, genetic algorithms are considered as the most effective ones

to address the wind farm layout optimization problems [41]. They excel in wind farm layout optimization by exploring a broad solution space efficiently, avoiding local optima and increasing the likelihood of finding superior layouts. Their adaptability allows simultaneous consideration of various constraints like turbine placement, wind patterns, and terrain limitations, ensuring flexible optimization. With the ability to handle uncertainties robustly, genetic algorithms are adept at accommodating real-world complexities, making them a valuable tool for wind farm layout design despite their need for computational resources and potential convergence challenges [42]. Nevertheless, genetic algorithms suffer from inefficient search capacity due to the premature mechanism. Recently, differential evolution (DE) algorithms have received increasing interests because they demonstrate robustness in handling complex, nonlinear objective functions, making them suitable for various real-world problems across different domains [43, 44]. DE's simplicity, ease of implementation, and ability to efficiently explore solution spaces while balancing between exploration and exploitation make it a popular choice for optimization, especially in scenarios where computational efficiency and reliable solutions are crucial [45–48]. To further improve the search efficiency for wind farm layout optimization problems, this paper proposes a novel binary genetic operator enhanced differential evolution algorithm, called LSHADE-SPAGA. By creatively integrating a binary genetic operator into a distinguished DE variant, namely LSHADE [49] with semi-parameter adaptation [50], LSHADE-SPAGA optimally leverages the global exploration capabilities of the binary genetic operator alongside the local exploitation proficiency of DE operators. This hybrid approach effectively balances search exploration and exploitation, aiming to yield superior solutions for wind farm layout optimization challenges. To assess LSHADE-SPAGA's effectiveness, comprehensive experiments have been carried out. The algorithm is tested across a variety of conditions, including four wind scenarios, twelve distinct layout constraints plus an unconstrained layout, and three types of turbines, totaling 156 test instances ($4 \times 13 = 156$). LSHADE-SPAGA is benchmarked against seven other cutting-edge algorithms. The experimental results demonstrate that LSHADE-SPAGA surpasses its competitors in terms of solution quality and the trade-off between convergence speed and accuracy.

The remainder of this paper is organized as follows: Section 2 presents an overview of wind farm layout optimization problems and introduces some notable optimization algorithms. Section 3 provides a detailed exposition of the proposed LSHADE-SPAGA method. Section 4 presents a comprehensive summary of the experimental results, encompassing comparative analyses and an ablation study of LSHADE-SPAGA. Finally, Section 5 concludes the paper with some general remarks and conclusions.

2. Related work

2.1. Representation of wind farm layout optimization problems

Wind farm layout optimization (WFLO) problems focus on strategically positioning wind turbines to maximize power generation while minimizing costs and environmental impacts. The core of these problems is an objective function that aims to minimize the ratio of total construction costs to the total power output of the wind farm. This involves optimizing the wind farm layout X and the number of turbines N. The total construction cost is quantified using a specific function, such as Mosetti's function [51], which takes into account the number of turbines and their arrangement. The optimization process also includes maximizing the total power output of the wind farm under various

wind conditions, which simplifies to maximizing the power output when the number of turbines is fixed. Each turbine's power output is calculated based on factors like wind speed, direction, and the layout configuration. Additionally, conversion efficiency is used to evaluate the wind farm's power generation performance, representing the efficiency of the turbine layout. A significant factor in WFLO is the wake effect, which refers to the reduction in wind speed and alteration in wind direction behind operating turbines. This effect can lead to decreased energy production and increased wear on downstream turbines. Models like Jensen's model [52] are used to estimate the wake velocity and its impact on the power output of other turbines in the farm. These optimization problems require balancing multiple factors to achieve an efficient and effective wind farm layout.

Mathematically, the goal of optimizing wind farm layout optimization is to enhance the power generation of a wind farm. This is achieved by developing an objective function expressed as

$$g = \text{minimize } \frac{T_{\text{cost}}}{\mathscr{W}_{\text{power}}} \tag{2.1}$$

where T_{cost} denotes the total construction cost of the wind farm, and $\mathscr{W}_{\text{power}}$ signifies the cumulative power output of the wind farm across various wind conditions. This optimization involves determining the wind farm layout X and the total number of wind turbines D.

To calculate the construction cost, Mosetti's function is employed, defined as

$$T_{\text{cost}} = D\left(\frac{2}{3} + \frac{1}{3}e^{-0.00174D^2}\right) \tag{2.2}$$

In our research, the number of wind turbines is fixed, simplifying the objective function (or fitness function for evaluating algorithmic solutions) to maximizing the overall power output of the wind farm under specific wind conditions ξ. This is represented as

$$g(X) = \text{maximize } \mathscr{W}_{\text{power}} = \sum_{i=1}^{D} \sum_{w,\lambda} p(w,\lambda)\mathcal{P}_i(w,\lambda,X) \tag{2.3}$$

where $\mathcal{P}_i(w,\lambda,X)$ is the power output of the ith turbine under wind speed w and direction λ in layout X, and $p(w,\lambda)$ is the probability distribution of wind speed and direction. Layout X is the decision variable in WFLO.

The power generation efficiency of a wind farm is assessed using a conversion efficiency η, defined as

$$\eta = \frac{\mathscr{W}_{\text{power}}}{D\sum_{w,\lambda}\mathcal{P}_r(w,\lambda,X)\cdot p(w,\lambda)} \tag{2.4}$$

where $\mathcal{P}_r(w,\lambda,X)$, without considering wake effects, represents the rated power of a turbine under specific wind conditions w and λ. A higher η value indicates a more efficient turbine layout.

The wake effect significantly influences a turbine's power output. It refers to the reduction in wind speed and directional changes caused by turbines, reducing downstream wind speed and affecting other turbines' efficiency in the same farm. This leads to energy production losses and increased turbulence and fatigue on downstream turbines. To assess wake velocity, Jensen's model is used, which predicts wind speed reduction and increased turbulence in a turbine's wake. This model assumes the wake as a cylindrical region expanding downstream from the turbine, with its diameter based on the

rotor's diameter and length dependent on various factors like wind speed and atmospheric conditions. The model calculates the wake's velocity deficit, which in turn is used to estimate the power output of downstream turbines and the overall energy production of the wind farm. Despite its simplicity, Jensen's model is effective in many wind farm scenarios [53–57].

2.2. Notable optimization algorithms

Several notable optimization algorithms have been developed for WFLO problems. In Grady et al. [26], a genetic algorithm approach is employed to optimize wind turbine placement, focusing on maximizing production capacity while reducing the number of turbines and land usage. The study examines three wind scenarios: unidirectional uniform wind, variable-direction uniform wind, and variable-direction non-uniform wind. For each scenario, 600 individuals are distributed among 20 subpopulations, evolving over 3000 or 2500 generations, depending on the scenario. The optimization results include optimal configurations, fitness levels, total power output, power output efficiency, and the turbine count per configuration. The study also reconciles differences with previous research and provides explanations for these discrepancies.

Gonzalez et al. [58] introduce an evolutionary algorithm for wind farm layout optimization, using a comprehensive cost model that accounts for initial investment, net cash flow over the wind farm's life, wind conditions, turbine features, and wake decay impact on energy production. The algorithm handles diverse terrain and constraints, such as limited land areas and investment caps, while focusing on minimizing production loss from wake decay. This advanced evolutionary algorithm has been favorably compared to prior results, demonstrating its effectiveness in various wind farm scenarios.

Abdelsalam et al. [59] propose an optimization method combining a binary real coded genetic algorithm with local search to enhance turbine placement in wind farms. Initially, this algorithm serves as the global optimization system, encoding potential turbine locations in a binary matrix and using a real matrix for power output calculations. This phase involves random initialization, fitness evaluation, reproduction via genetic operators, and repairing infeasible individuals. The local search phase then refines this approximate solution, improving solution quality by exploring the solution's local region. The method is designed to terminate upon reaching a predefined number of generations or achieving convergence, with the overall goal of optimizing the efficiency of wake interaction among turbines.

More recent advancements include two state-of-the-art genetic algorithms proposed in Ju et al. [41, 42]. The first, an adaptive genetic algorithm (AGA) [41], incorporates a self-awareness mechanism allowing chromosomes to evaluate turbine efficiency and target improvements, initially relocating the least efficient turbine randomly. Extensive tests confirm AGA's superiority over conventional genetic algorithms in wind farm layout optimization. The second, a support vector regression (SVR) guided genetic algorithm (SUGGA) [42], integrates self-adjustment capabilities with an SVR-based response surface guidance for turbine relocation, assessing landowner participation constraints on farm efficiency. SUGGA outperforms baseline algorithms in various scenarios, providing significant efficiency improvements and insights for wind farm planning.

A comprehensive study by Kunakote et al. [37] bridges metaheuristics with wind farm layout design, assessing twelve metaheuristic algorithms in WFLO. The study formulates four WFLO problems, with goals to minimize costs and maximize power production, varying turbine placement and numbers. Employing Jansen's wake model and two energy estimation methods, the study compares metaheuristics for convergence and consistency. It identifies the moth-flame optimization

algorithm as the most efficient, setting a benchmark for future metaheuristic studies in WFLO.

Despite these advancements, the No-Free-Lunch theorem [60] suggests that these algorithms, including genetic algorithms and metaheuristics, still face limitations in search efficiency across diverse wind scenarios. This limitation underscores the ongoing need for more efficient algorithms to tackle the complexities of WFLO.

3. Proposed LSHADE-SPAGA method

In this study, we introduce for the first time an efficient optimization algorithm for WFLO problems, which innovatively integrates novel binary genetic operators with a notable DE variant, namely LSHADE with semi-parameter adaptation [50] (LSHADE-SPA). The original LSHADE algorithm [49], an advanced version of DE [61], is renowned for its adaptive control parameters and success-history based approach, employing a limited memory strategy to dynamically adjust the scaling factor and crossover rate. This enhances its flexibility and efficiency, particularly in reducing the population size during the optimization process to refine solutions. LSHADE is exceptionally effective in multi-modal and high-dimensional challenges, adeptly balancing exploration and exploitation to avoid local optima and seek global solutions. LSHADE-SPA further elevates LSHADE by introducing a semi-parameter adaptation method, which strikes a balance between random, fully adaptive, and self-adaptive algorithms. In our newly proposed LSHADE-SPAGA, we have developed two unique binary mutation and crossover operators, specifically tailored for optimizing wind farm layouts.

Mathematically, the population $\mathbf{X}$ in the LSHADE-SPAGA method can be represented as

$$\begin{aligned} &\mathbf{X} = \{X_1, X_2, ..., X_N\}, \\ &X_i = \{x_i^1, x_i^2, ..., x_i^D\} \end{aligned} \tag{3.1}$$

where N is the size of the population, and D denotes the dimension of WFLO problems, corresponding to the number of turbines placed in the wind farm. In this study, an integer coding strategy is proposed to construct a wind farm, which makes the dimension of problems equal to the number of wind turbines in the wind farm. Importantly, x_i^d is an integer value that signifies the position of each turbine within the wind farm.

Upon generating N feasible solutions randomly, we specifically design a novel binary genetic mutation operator tailored for wind farm layout optimization, formulated as

$$x_i^d = \begin{cases} \text{Randi}(1, M), & \text{if } r < p_m \\ x_i^d, & \text{otherwise} \end{cases} \tag{3.2}$$

where $\text{Randi}(1, M)$ randomly selects an integer from the interval $[1, M]$. It is important to note that the layout for a WFLO problem is discretely segmented into various grids, each representing potential turbine placement locations. For example, in our experiments, the wind farm layout comprises $M = 12 \times 12$ such locations. Here, M signifies the maximum possible position for wind turbines within the wind farm, r is a random number drawn from a uniform distribution between 0 and 1, and p_m represents the mutation probability.

To facilitate frequent information exchange among different individuals in the LSHADE-SPAGA method, we have designed a binary crossover operation, which is formulated as

$$U_i = \begin{cases} \{x_i^1, ..., x_i^d, x_j^{d+1}, ..., x_j^D\} & \text{if} \quad r < p_c \\ X_i, & \text{otherwise} \end{cases} \\ \text{s.t.} \quad x_i^d < x_j^{d+1} \tag{3.3}$$

where U_i represents a new individual created through the crossover operator. i and j are indices randomly selected from the interval $[1, N]$, d is a randomly chosen crossover point, and p_c is the crossover probability. Notably, the indices of wind turbines in an individual are sorted in ascending order. Because a fixed number of wind turbines are used in this study, we restrict the location of wind turbines at the crossover point to guarantee that the number of wind turbines does not change during the crossover operation.

Individuals that have undergone genetic mutation and crossover are then subject to differential mutation, described by

$$X_i = X_i + F(X_{best} - X_i) + F(X_{r1} - X_{r2}) \tag{3.4}$$

where X_{best} is the best individual in the current population, and X_{r1} and X_{r2} are distinct individuals randomly selected from the population, distinct from each other and from X_i. F is a scaling factor that influences the rate of mutation.

Additionally, LSHADE-SPAGA incorporates a linear population size reduction strategy [49] to dynamically adjust its population size. This is described mathematically as:

$$N = \text{round}\left(\frac{N_{min} - N_{max}}{MaxNEF} * NEF + N_{max}\right) \tag{3.5}$$

where N_{min} and N_{max} represent the minimum and maximum population sizes, respectively. NEF is the current number of fitness evaluations, and MaxNEF is the predefined maximum number of fitness evaluations. The round function is used to round the result to the nearest integer. This formula effectively adjusts the population size based on the progress of the optimization process, maintaining an optimal balance between exploration and exploitation as the algorithm evolves.

In LSHADE-SPAGA, the selection between genetic operator mutations and differential evolution updates for individuals is determined by a memory probability

$$X_i = \begin{cases} (3.2) & \text{if} \quad H_i < r \\ (3.4) & \text{otherwise} \end{cases} \tag{3.6}$$

where H_i represents the memory probability of individual X_i, initially set to 0.5 for each individual. This memory probability is updated as

$$w = g(\mathbf{X}') - g(\mathbf{X}); \\ H = H * L - (1 - L) * \frac{\sum_{i \in better} w_i}{\text{sum}(w)} \tag{3.7}$$

where L being the learning rate, set to 0.8. Here, g is the fitness evaluation function defined in Eq (2.1), and w is the fitness difference between parent $\mathbf{X}$ and offspring $\mathbf{X}'$. The proportion of better-performing

individuals is used to adjust H, which is constrained within the range $(0.2, 0.8)$ to maintain balance:

$$H = \begin{cases} 0.2, & H < 0.2 \\ 0.8, & H > 0.8 \\ H, & \text{otherwise} \end{cases} \tag{3.8}$$

After mutation, LSHADE-SPAGA replaces the original LSHADE crossover operator with the binary crossover operator (3.3). Additionally, an adaptive strategy is employed to adjust the scaling factor F, enhancing performance.

$$\begin{aligned} F_i &= 0.45 + 0.1r \\ F_i &= \text{randc}(MF_i, \delta) \end{aligned} \tag{3.9}$$

where randc$(\cdot)$ represents the Cauchy distribution, MF_i is a randomly selected memory slot storing successful means from previous generations, and δ is the standard deviation of the Cauchy distribution. This adaptive approach contributes to the overall efficiency and effectiveness of the algorithm in optimizing the wind farm layout.

The processes of the proposed algorithms include initialization, crossover, mutation, and selection operations. Assuming that there are D wind turbines in a wind farm. The time complexity of initialization is $O(ND)$, where N is the population size. The crossover and mutation of LSHADE requires $O(ND)$. The mutation and crossover operations with the sorted operation of GA both have computational complexity $O(ND) + O(N \log D)$ in the worst case. Then, the parameters update of LSHADE requires $O(2N)$. The complexity of evaluating function is $O(ND)$. Finally, the selection is $O(N)$. As a result, the overall time complexity of DCADE in the worst case is $O(ND)$.

4. Experimental results and discussions

4.1. Experiment setting

To thoroughly evaluate the efficacy of the LSHADE-SPAGA algorithm, extensive experiments were conducted. Figure 1 presents wind roses for four distinct wind scenarios, which visually represent the distribution of wind frequencies from various directions. Specifically, wind scenario 1 is characterized by a single, predominant wind direction from the North (N), indicated by a 100% frequency, signifying a consistent northerly wind. Wind scenario 2 exhibits a range of wind directions with a notable frequency from the North, varying between 5% and 25%. Wind scenario 3 shows a more balanced spread of directions, with the highest frequency being 30% from the North, decreasing in a clockwise direction. Wind scenario 4 displays the greatest diversity in wind directions, with frequencies evenly distributed and not surpassing 9% for any direction. The wind roses also differentiate wind speeds using color coding: dark red represents 13 m/s, orange denotes 10 m/s, and light green indicates 7 m/s. The segment lengths in each direction are proportional to the frequency of wind at those respective speeds and directions.

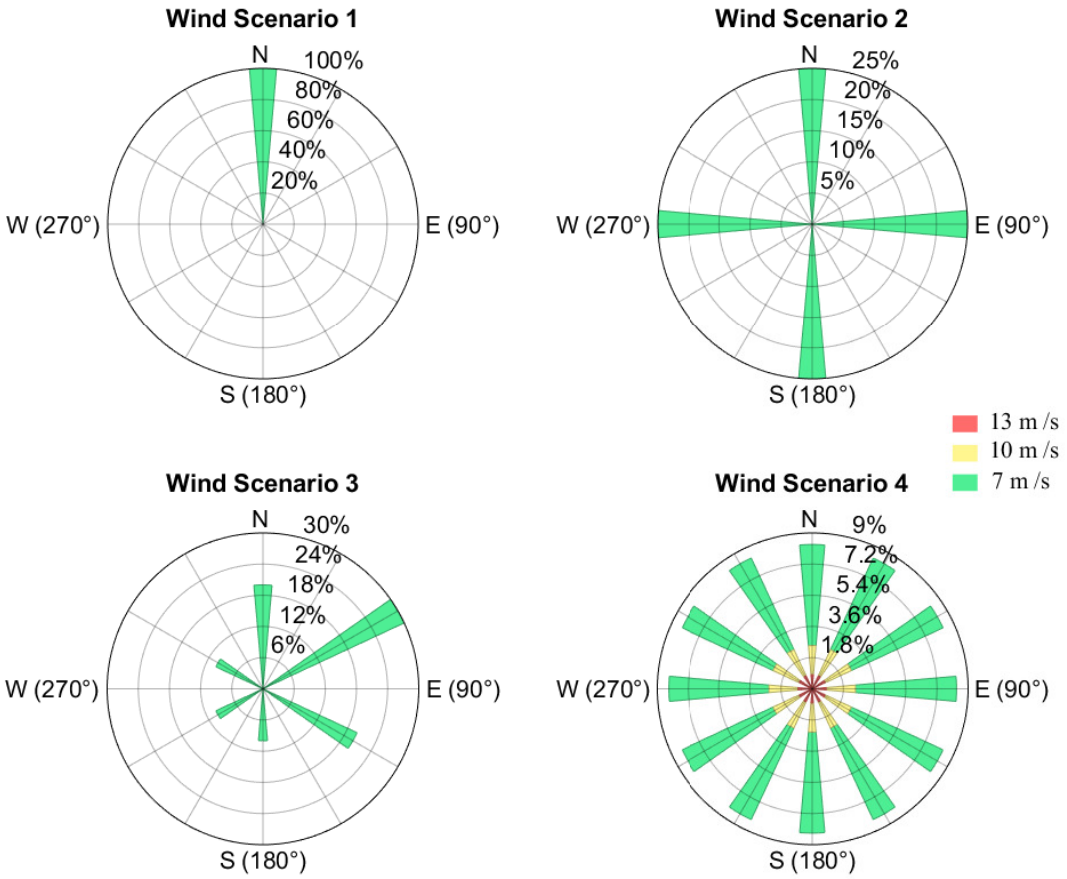

Figure 1. The wind roses used in the experiments.

Figure 2 displays a matrix layout consisting of twelve smaller matrices, each labeled with a constraint from L_1 to L_{12}. These matrices represent different topographical constraints for a given area for wind farm layout optimization. Each cell within the matrices is numbered sequentially from 1 to 144, representing individual possible locations for wind turbines. The matrices under each constraint have certain cells shaded in purple, indicating areas where placing turbines is not feasible due to the specific topographical constraints of that scenario. The arrangement and number of shaded cells vary across the constraints, suggesting unique topographical features or limitations for each scenario. Figure 2 illustrates how various topographical constraints can impact the available space for turbine placement in wind farm layout planning.

To evaluate the performance of the proposed LSHADE-SPAGA methods, eight state-of-the-art optimization algorithms are used as competitors, including: nonlinear programming (NLP), SHADE [62], LSHADE [49], LSHADE-SPACMA [50], CJADE [63], CMA-ES [64], AGA [41], and SUGGA [42]. SHADE is an enhanced version of the DE algorithm that uses historical success rates to adjust its strategy parameters dynamically. LSHADE is a variant of SHADE that incorporates a limited memory mechanism to further refine the adaptive parameter adjustment process. LSHADE-SPACMA is a hybrid method that combines LSHADE with a semi-parameter adaptation

and the covariance matrix adaptation evolution strategy to improve exploration and exploitation capabilities. CJADE is an iteration of the DE algorithm that integrates chaotic maps to maintain diversity in the population and avoid premature convergence. CMA-ES is a strategy that uses a statistical model of the candidate solutions' distribution to guide the search for the global optimum. AGA is a genetic algorithm that adapts its parameters based on the observed performance of the population, allowing for self-adjustment in response to the optimization challenge. SUGGA is an algorithm that employs support vector regression as a surrogate model to inform the genetic algorithm's search process, aiming to improve precision in the placement of wind turbines. Each of these algorithms incorporates different mechanisms to handle complex optimization problems, making them suitable competitors for evaluating the performance of LSHADE-SPAGA in various wind farm layout optimization scenarios.

Figure 2. The constraint of different topographies.

4.2. Experimental results

Tables 1–4 present a comprehensive comparison of the performance of various algorithms under four distinct wind scenarios. The most favorable outcomes across all the algorithms are denoted in bold for emphasis. Each table includes the mean and standard deviation values of conversion efficiency, the mean value of different constraints, and Wilcoxon signed-rank test results. Each table is categorized into three principal sections based on the number of turbines: 15, 20, and 25. Within these sections, the algorithms' performances are assessed against a series of constraints, designated from L_0 to L_{12}. Here L_0 denotes an unconstrained layout, while L_1 to L_{12} correspond to the constraints depicted in Figure 2. The algorithms' effectiveness is quantified by the average power output they produce, with each value accompanied by its standard deviation in parentheses to indicate variability.

The data from these tables clearly demonstrate that the proposed LSHADE-SPAGA algorithm secures the highest number of optimal results across different wind scenarios: achieving the best outcomes in 24 out of 36 instances for wind scenario 1, in 30 out of 36 instances for wind scenario 2, in 34 out of 36 instances for wind scenario 3, and in all 36 instances for wind scenario 4. LSHADE-SPAGA achieves the best average values in 11 out of 12 groups, with the only exception being the case of 15 turbines under wind scenario 1. These findings indicate that LSHADE-SPAGA consistently surpasses its counterparts in terms of solution quality. Furthermore, as the complexity of the WFLO problem escalates from scenario 1 to scenario 4, LSHADE-SPAGA not only maintains performance but actually shows improved results, suggesting its superior capability to tackle increasingly complex problems. Additionally, the significance of these results is backed by p-values, most of which are below the 0.05 threshold, providing statistical evidence that LSHADE-SPAGA significantly outperforms the competing algorithms. Notably, Although LSHADE-SPAGA can not obtain better results than SUGGA in small-scale wind farms, it also gets the same quality solution in this situation and has the best conversion efficiency in middle and large-scale wind farms. The Wilcoxon results have demonstrated that LSHADE-SPAGA is significantly better than its competitors. Compared with the mathematical method, all meta-heuristic algorithms perform better than it. NLP performs an unstable performance under different constraints, while LSHADE-SPAGA is able to obtain stable solutions than other methods.

For a deeper understanding of the search dynamics of the proposed algorithm, Figures 3–6 present convergence plots. Each figure includes three convergence graphs for varying turbine counts: 15, 20, and 25. These graphs chart the improvement of conversion efficiency against the number of function evaluations, which is a standard metric for gauging optimization algorithm performance. All tested algorithms are benchmarked, including AGA, SUGGA, SHADE, CMA-ES, CJADE, LSHADE, LSHADE-SPACMA, and LSHADE-SPAGA. The y-axis quantifies conversion efficiency, reflecting the turbines' ability to convert wind to energy, and the x-axis tracks the total function evaluations, indicative of the computational investment of the optimization. Generally, as function evaluations climb, so does efficiency, underscoring typical optimization convergence. With an increase in turbines, more evaluations are needed for convergence, and a ceiling of $10000D$ function evaluations is set. These plots show that, while LSHADE-SPACMA's convergence rate is moderate, it ultimately outperforms other algorithms in achieving superior conversion efficiency, showcasing its adeptness at balancing global exploration and local exploitation.

Table 1. Performance comparison results of all algorithms under wind scenario 1.

Turbine		NLP	AGA	SUGGA	SHADE	CJADE	CMAES	LSHADE	LSHADE-SPACMA	LSHADE-SPAGA
	L0	80.16	97.58(0.14)	97.76(0.12)	97.66(0.13)	97.43(0.17)	96.20(1.21)	96.84(0.49)	96.59(0.50)	**97.82(0.12)**
	L1	74.03	97.00(0.25)	**97.14(0.21)**	96.71(0.17)	96.56(0.20)	94.90(1.73)	95.84(0.60)	95.60(0.52)	96.91(0.11)
	L2	79.05	97.69(0.12)	97.79(0.11)	97.79(0.09)	97.68(0.12)	96.94(0.87)	97.32(0.30)	97.03(0.39)	**97.85(0.07)**
	L3	84.88	97.14(0.67)	**97.70(0.25)**	95.58(0.32)	95.13(0.29)	93.57(1.34)	94.54(0.75)	93.82(0.61)	96.16(0.22)
	L4	72.08	97.20(0.57)	**97.41(0.42)**	95.50(0.36)	95.01(0.31)	92.72(1.39)	94.30(0.71)	93.85(0.76)	96.11(0.27)
	L5	87.74	97.71(0.10)	97.80(0.09)	97.84(0.07)	97.75(0.11)	96.17(1.82)	97.44(0.27)	97.00(0.39)	**97.87(0.06)**
15	L6	81.03	97.44(0.22)	97.73(0.12)	97.32(0.38)	97.18(0.23)	95.78(1.76)	96.15(0.64)	95.92(0.68)	**97.78(0.14)**
	L7	72.15	97.31(0.16)	**97.47(0.14)**	97.19(0.18)	96.99(0.18)	96.40(0.66)	96.30(0.57)	96.05(0.49)	97.42(0.10)
	L8	75.94	97.59(0.13)	97.76(0.10)	97.73(0.11)	97.59(0.13)	96.70(0.77)	97.24(0.36)	96.84(0.32)	**97.84(0.09)**
	L9	81.70	97.50(0.34)	**97.70(0.21)**	96.72(0.25)	96.36(0.20)	94.90(1.30)	95.68(0.57)	95.35(0.65)	97.00(0.15)
	L10	67.54	97.45(0.37)	**97.53(0.34)**	96.66(0.24)	96.23(0.29)	94.31(1.62)	95.68(0.53)	95.31(0.54)	96.99(0.15)
	L11	84.17	97.66(0.13)	97.78(0.10)	97.79(0.11)	97.65(0.09)	95.90(2.06)	97.15(0.43)	96.79(0.41)	**97.86(0.07)**
	L12	67.76	97.45(0.22)	97.66(0.14)	97.33(0.40)	97.09(0.21)	96.43(1.21)	96.23(0.63)	96.13(0.61)	**97.76(0.14)**
Average		77.56	97.44(0.26)	**97.63(0.18)**	97.06(0.22)	96.82(0.19)	95.46(1.36)	96.21(0.53)	95.87(0.53)	97.33(0.13)
p-value		1.22E-04	5.54E-01	7.73E-01	1.22E-04	1.22E-04	1.22E-04	1.22E-04	1.22E-04	–
	L0	75.22	93.52(0.47)	94.10(0.36)	93.54(0.62)	92.84(0.36)	90.13(1.63)	91.51(1.12)	90.14(0.79)	**94.93(0.43)**
	L1	73.12	91.88(0.62)	92.36(0.62)	91.85(0.49)	90.85(0.42)	87.21(1.81)	89.37(1.10)	88.31(0.99)	**93.24(0.35)**
	L2	71.00	94.04(0.32)	94.47(0.37)	94.64(0.52)	94.07(0.25)	91.16(1.67)	92.94(0.88)	91.79(0.98)	**95.08(0.30)**
	L3	63.92	92.55(0.77)	**93.77(0.65)**	90.40(0.80)	89.08(0.49)	85.00(1.75)	87.26(1.15)	85.97(0.86)	92.54(0.85)
	L4	64.88	92.82(0.95)	**93.25(1.05)**	90.30(0.90)	88.99(0.53)	85.49(1.81)	87.27(1.42)	85.88(1.08)	92.64(0.73)
	L5	65.75	94.11(0.39)	94.60(0.28)	94.89(0.39)	94.34(0.20)	90.37(2.00)	93.20(1.06)	91.80(1.06)	**95.28(0.30)**
20	L6	75.58	92.17(0.82)	92.96(0.55)	91.56(0.42)	90.82(0.45)	89.08(1.39)	88.24(1.09)	88.26(0.99)	**93.55(0.67)**
	L7	72.90	92.73(0.50)	93.35(0.54)	92.91(0.49)	91.92(0.38)	88.21(1.91)	90.42(1.14)	89.10(1.01)	**94.03(0.42)**
	L8	81.16	93.79(0.47)	94.29(0.28)	94.35(0.29)	93.64(0.28)	91.51(1.62)	92.66(0.92)	91.08(0.93)	**95.01(0.30)**
	L9	68.97	93.20(0.73)	94.05(0.40)	92.41(0.51)	91.33(0.42)	88.04(2.46)	89.74(1.23)	88.15(0.79)	**94.11(0.58)**
	L10	69.84	92.99(0.59)	93.53(0.75)	92.20(0.43)	91.18(0.49)	88.41(1.51)	89.69(1.25)	88.38(1.01)	**93.91(0.54)**
	L11	80.60	93.80(0.47)	94.36(0.32)	94.43(0.64)	93.82(0.30)	89.71(2.23)	92.50(1.22)	90.68(0.96)	**95.09(0.38)**
	L12	62.68	92.79(0.53)	93.48(0.48)	92.53(0.51)	91.66(0.41)	88.71(1.71)	89.85(1.22)	89.02(0.96)	**94.13(0.53)**
Average		71.20	93.11(0.59)	93.74(0.51)	92.77(0.54)	91.89(0.38)	88.69(1.81)	90.36(1.14)	89.12(0.96)	**94.12(0.49)**
p-value		1.22E-04	6.10E-04	2.39E-02	1.22E-04	1.22E-04	1.22E-04	1.22E-04	1.22E-04	–
	L0	72.59	87.54(0.62)	88.43(0.65)	88.53(0.47)	87.41(0.42)	83.90(1.86)	85.29(1.27)	83.53(0.97)	**90.63(0.67)**
	L1	65.69	85.23(0.59)	85.94(0.85)	85.74(0.57)	84.51(0.44)	80.01(1.94)	82.41(1.51)	80.69(0.97)	**88.13(0.81)**
	L2	68.16	88.21(0.70)	88.84(0.50)	90.21(0.37)	89.13(0.36)	85.25(1.93)	86.51(1.58)	84.76(0.83)	**91.00(0.61)**
	L3	64.58	86.36(1.04)	**87.90(1.21)**	82.72(0.53)	81.68(0.43)	78.04(1.87)	79.58(1.38)	77.59(0.73)	84.14(0.50)
	L4	61.75	86.13(1.09)	**86.63(1.21)**	82.74(0.44)	81.40(0.47)	77.86(1.45)	79.30(1.22)	77.78(1.02)	84.09(0.51)
	L5	61.65	88.30(0.56)	89.03(0.71)	90.49(0.56)	89.40(0.32)	84.90(1.80)	87.00(1.63)	84.58(1.09)	**91.33(0.54)**
25	L6	70.35	85.25(0.76)	86.30(0.73)	84.94(0.36)	84.14(0.47)	81.21(1.11)	80.94(1.35)	79.86(0.72)	**87.22(0.54)**
	L7	72.12	86.37(0.49)	87.35(0.75)	87.31(0.54)	85.97(0.50)	82.37(1.53)	83.65(1.40)	81.88(1.09)	**89.56(0.68)**
	L8	70.95	87.87(0.62)	88.73(0.65)	89.65(0.38)	88.37(0.32)	84.46(1.52)	86.31(1.46)	84.24(0.97)	**90.85(0.60)**
	L9	68.26	86.85(0.80)	**88.18(0.71)**	85.96(0.45)	84.67(0.45)	80.92(1.57)	82.49(1.36)	80.88(0.84)	87.54(0.57)
	L10	65.47	87.16(0.99)	**87.78(0.98)**	85.92(0.43)	84.61(0.29)	81.27(2.09)	82.49(1.11)	80.82(0.81)	87.41(0.52)
	L11	65.57	87.84(0.62)	88.81(0.62)	89.67(0.75)	88.61(0.38)	84.81(1.62)	86.55(1.35)	83.90(1.00)	**91.01(0.63)**
	L12	72.41	86.24(0.58)	87.28(0.56)	86.83(0.47)	85.62(0.44)	82.74(1.59)	82.87(1.63)	81.61(0.99)	**89.00(0.76)**
Average		67.66	86.87(0.73)	87.78(0.78)	86.98(0.49)	85.81(0.41)	82.13(1.68)	83.49(1.40)	81.70(0.93)	**88.61(0.61)**
p-value		1.22E-04	4.03E-03	1.22E-01	1.22E-04	1.22E-04	1.22E-04	1.22E-04	1.22E-04	–

Table 2. Performance comparison results of all algorithms under wind scenario 2.

Turbine		NLP	AGA	SUGGA	SHADE	CJADE	CMAES	LSHADE	LSHADE-SPACMA	LSHADE-SPAGA
	L0	84.27	95.31(0.43)	95.29(0.42)	95.93(0.62)	96.20(0.37)	92.63(2.19)	95.16(0.79)	93.88(0.73)	**96.97(0.35)**
	L1	68.54	94.79(0.72)	**95.02(0.68)**	93.82(0.47)	94.06(0.32)	89.88(2.28)	92.87(0.87)	91.54(0.73)	94.69(0.35)
	L2	81.89	94.62(0.57)	94.60(0.63)	94.60(0.52)	94.83(0.38)	91.30(1.96)	93.74(0.72)	92.29(0.70)	**95.40(0.31)**
	L3	77.34	95.01(0.70)	**95.10(0.49)**	93.61(0.65)	94.06(0.37)	90.46(1.67)	92.52(0.93)	91.26(0.84)	94.71(0.37)
	L4	76.92	94.75(0.53)	94.41(0.59)	94.59(0.46)	94.68(0.31)	92.19(1.53)	93.02(0.95)	92.08(0.68)	**95.33(0.29)**
	L5	81.37	94.68(0.49)	94.53(0.47)	95.11(0.69)	95.33(0.38)	92.95(1.23)	93.85(0.86)	92.59(0.60)	**96.38(0.34)**
15	L6	82.27	94.91(0.39)	95.11(0.44)	95.74(0.62)	95.81(0.47)	92.00(2.16)	94.31(0.99)	92.88(0.88)	**96.51(0.29)**
	L7	78.71	95.23(0.52)	95.47(0.50)	94.97(0.53)	95.31(0.36)	91.20(1.92)	94.20(0.84)	92.93(0.76)	**95.82(0.35)**
	L8	80.94	94.97(0.58)	94.95(0.58)	95.45(0.46)	95.59(0.38)	91.30(2.12)	94.34(0.82)	93.21(0.70)	**96.23(0.41)**
	L9	79.53	95.09(0.64)	95.34(0.52)	95.02(0.38)	95.25(0.39)	91.50(1.92)	93.90(0.95)	92.50(0.68)	**95.91(0.41)**
	L10	81.78	95.09(0.59)	94.97(0.42)	95.43(0.42)	95.61(0.39)	92.25(1.39)	94.17(0.97)	92.91(0.73)	**96.14(0.37)**
	L11	81.78	95.06(0.44)	95.05(0.47)	95.90(0.48)	96.10(0.36)	92.34(1.71)	94.54(0.82)	93.48(0.85)	**96.70(0.32)**
	L12	77.68	95.11(0.41)	95.12(0.40)	95.72(0.53)	96.11(0.39)	92.00(1.95)	94.86(0.90)	93.48(0.68)	**96.54(0.30)**
Average		79.46	94.97(0.54)	95.00(0.51)	95.07(0.53)	95.30(0.37)	91.69(1.85)	93.96(0.88)	92.69(0.74)	**95.95(0.34)**
p-value		1.22E-04	6.10E-04	8.54E-04	1.22E-04	1.22E-04	1.22E-04	1.22E-04	1.22E-04	–
	L0	79.43	88.72(0.47)	88.75(0.51)	89.82(0.61)	90.21(0.36)	86.20(1.86)	88.60(0.96)	86.73(0.88)	**90.90(0.45)**
	L1	72.37	87.57(0.83)	**88.02(0.81)**	86.31(0.67)	86.73(0.34)	82.86(1.58)	84.84(0.98)	83.32(0.93)	87.06(0.50)
	L2	69.02	88.01(0.77)	87.97(0.73)	88.21(0.53)	88.51(0.33)	84.54(1.54)	86.27(1.20)	84.76(0.73)	**89.00(0.39)**
	L3	64.88	88.02(0.88)	**88.47(0.60)**	86.16(0.75)	86.65(0.32)	83.67(1.74)	84.45(0.99)	82.95(0.90)	87.24(0.40)
	L4	66.71	88.33(0.54)	88.08(0.73)	88.32(0.49)	88.61(0.30)	85.35(1.27)	86.11(1.04)	84.45(0.72)	**88.89(0.38)**
	L5	76.11	88.00(0.49)	87.88(0.57)	88.73(0.39)	88.97(0.28)	86.07(1.34)	86.88(1.07)	85.22(0.69)	**89.68(0.41)**
20	L6	66.88	88.22(0.50)	88.24(0.48)	88.49(0.54)	88.67(0.30)	84.69(1.77)	86.37(0.97)	84.84(1.03)	**89.61(0.40)**
	L7	73.02	88.53(0.67)	88.46(0.59)	88.15(0.73)	88.62(0.27)	84.35(1.85)	86.73(1.01)	85.18(0.95)	**89.26(0.39)**
	L8	74.64	88.40(0.55)	88.43(0.66)	89.19(0.79)	89.64(0.42)	85.52(1.80)	87.71(1.14)	85.76(0.87)	**90.12(0.48)**
	L9	72.97	88.35(0.76)	88.46(0.52)	88.31(0.59)	88.62(0.38)	85.51(1.51)	86.56(1.16)	84.85(0.67)	**89.22(0.41)**
	L10	77.46	88.56(0.54)	88.36(0.66)	89.04(0.66)	89.41(0.34)	85.95(1.35)	87.38(1.08)	85.44(0.73)	**90.07(0.41)**
	L11	78.60	88.54(0.52)	88.33(0.40)	89.68(0.55)	89.81(0.33)	86.73(1.37)	87.68(1.10)	86.21(0.75)	**90.46(0.39)**
	L12	68.71	88.69(0.51)	88.71(0.52)	89.21(0.78)	89.44(0.36)	85.57(1.27)	87.31(0.89)	85.89(0.78)	**90.39(0.44)**
Average		72.37	88.30(0.62)	88.32(0.60)	88.43(0.62)	88.76(0.33)	85.15(1.56)	86.68(1.05)	85.05(0.82)	**89.38(0.42)**
p-value		1.22E-04	1.22E-03	5.25E-03	1.22E-04	1.22E-04	1.22E-04	1.22E-04	1.22E-04	–
	L0	67.25	81.91(0.37)	81.95(0.46)	83.28(0.67)	83.75(0.34)	80.14(1.28)	82.04(0.98)	79.86(0.79)	**84.25(0.40)**
	L1	64.03	80.38(0.85)	**80.66(0.90)**	78.66(0.59)	79.02(0.29)	75.94(1.05)	77.16(0.71)	75.40(0.67)	79.45(0.36)
	L2	71.63	81.29(0.77)	81.08(0.63)	81.54(0.39)	81.54(0.31)	77.68(1.33)	79.21(1.12)	77.33(0.75)	**81.98(0.39)**
	L3	59.83	81.09(0.72)	**81.45(0.70)**	79.03(0.36)	78.97(0.30)	76.43(1.08)	76.56(0.85)	74.97(0.55)	79.50(0.40)
	L4	67.38	81.42(0.62)	81.36(0.72)	81.42(0.37)	81.58(0.33)	78.21(1.14)	78.96(1.07)	77.20(0.86)	**82.05(0.33)**
	L5	64.91	81.60(0.41)	81.26(0.38)	82.67(0.40)	82.70(0.26)	79.69(1.31)	80.28(0.97)	78.35(0.63)	**83.39(0.32)**
25	L6	64.72	81.35(0.50)	81.52(0.60)	81.67(0.60)	81.73(0.39)	77.47(1.36)	78.84(1.17)	77.04(0.70)	**82.78(0.37)**
	L7	62.72	81.53(0.54)	81.65(0.73)	81.01(0.70)	81.54(0.28)	78.43(1.38)	79.51(1.06)	77.79(0.57)	**82.05(0.41)**
	L8	60.37	81.73(0.59)	81.43(0.58)	82.42(0.59)	82.76(0.25)	79.33(1.19)	80.51(0.91)	78.49(0.67)	**83.07(0.40)**
	L9	71.35	81.51(0.61)	81.80(0.71)	81.19(0.81)	81.54(0.25)	77.98(1.19)	79.06(0.96)	77.48(0.69)	**82.06(0.41)**
	L10	71.17	81.71(0.72)	81.64(0.53)	82.56(0.66)	82.77(0.30)	79.57(1.29)	80.34(0.99)	78.54(0.76)	**83.20(0.43)**
	L11	68.13	81.98(0.52)	81.79(0.37)	83.13(0.64)	83.48(0.28)	80.26(1.19)	80.99(0.89)	79.25(0.76)	**83.99(0.35)**
	L12	72.28	81.85(0.40)	81.85(0.36)	82.57(0.86)	82.96(0.48)	78.70(1.36)	80.76(1.12)	78.61(0.74)	**83.76(0.39)**
Average		72.28	81.49(0.59)	81.50(0.59)	81.63(0.59)	81.87(0.31)	78.45(1.24)	79.56(0.98)	77.72(0.70)	**82.43(0.38)**
p-value		1.22E-04	1.33E-02	1.64E-02	1.22E-04	1.22E-04	1.22E-04	1.22E-04	1.22E-04	–

Table 3. Performance comparison results of all algorithms under wind scenario 3.

Turbine		NLP	AGA	SUGGA	SHADE	CJADE	CMAES	LSHADE	LSHADE-SPACMA	LSHADE-SPAGA
	L0	87.38	98.52(0.25)	98.85(0.22)	98.46(0.32)	98.25(0.35)	96.04(1.19)	97.46(0.69)	96.63(0.57)	**99.26(0.14)**
	L1	84.33	98.05(0.34)	98.31(0.28)	98.01(0.37)	97.60(0.36)	95.12(1.32)	97.11(0.85)	95.63(0.54)	**99.00(0.18)**
	L2	90.18	98.72(0.26)	98.98(0.19)	98.83(0.25)	98.78(0.23)	96.63(1.16)	98.08(0.53)	96.96(0.48)	**99.27(0.10)**
	L3	84.63	98.22(0.38)	**98.82(0.29)**	97.66(0.42)	97.38(0.29)	94.93(1.58)	96.54(0.79)	95.61(0.53)	98.72(0.23)
	L4	84.28	98.19(0.38)	98.51(0.31)	97.86(0.38)	97.50(0.25)	95.10(0.97)	96.64(0.69)	95.91(0.66)	**98.72(0.17)**
	L5	86.70	98.72(0.25)	98.99(0.20)	98.81(0.27)	98.60(0.26)	95.65(1.42)	98.18(0.58)	97.19(0.50)	**99.26(0.12)**
15	L6	83.78	97.99(0.36)	98.49(0.30)	97.57(0.52)	97.58(0.39)	95.67(1.48)	96.04(0.72)	95.49(0.59)	**98.98(0.27)**
	L7	91.44	98.32(0.34)	98.66(0.23)	98.21(0.37)	97.94(0.34)	95.45(1.30)	97.28(0.77)	96.15(0.48)	**99.08(0.16)**
	L8	85.73	98.57(0.27)	98.98(0.18)	98.65(0.44)	98.44(0.31)	96.90(0.98)	97.71(0.64)	96.81(0.53)	**99.26(0.10)**
	L9	85.88	98.42(0.38)	98.91(0.28)	98.13(0.37)	97.89(0.37)	95.30(1.15)	96.92(0.75)	96.15(0.70)	**98.98(0.16)**
	L10	86.96	98.34(0.28)	98.76(0.24)	98.02(0.41)	97.90(0.32)	94.95(1.61)	97.06(0.68)	96.20(0.53)	**98.99(0.18)**
	L11	90.65	98.64(0.25)	98.94(0.22)	98.73(0.31)	98.47(0.28)	97.06(1.28)	97.79(0.66)	96.92(0.45)	**99.27(0.12)**
	L12	84.96	98.09(0.32)	98.37(0.34)	97.95(0.37)	97.73(0.29)	95.98(1.93)	96.73(0.75)	95.86(0.50)	**98.99(0.20)**
Average		86.68	98.37(0.31)	98.74(0.25)	98.22(0.37)	98.00(0.31)	95.75(1.34)	97.20(0.70)	96.27(0.54)	**99.06(0.16)**
p-value		1.22E-04	1.22E-04	3.66E-04	1.22E-04	1.22E-04	1.22E-04	1.22E-04	1.22E-04	–
	L0	84.60	96.37(0.42)	97.10(0.41)	96.10(0.46)	95.59(0.39)	92.52(1.58)	94.36(0.76)	92.68(0.72)	**97.90(0.54)**
	L1	79.06	95.41(0.57)	95.98(0.48)	94.95(0.50)	94.29(0.43)	91.24(1.63)	93.74(0.97)	91.62(0.68)	**97.52(0.59)**
	L2	84.70	96.51(0.37)	97.07(0.35)	96.78(0.47)	96.22(0.35)	92.87(1.21)	94.95(0.97)	93.37(0.64)	**98.08(0.38)**
	L3	78.58	95.66(0.58)	**96.95(0.49)**	94.82(0.46)	94.23(0.39)	90.94(1.21)	93.18(1.09)	91.17(0.64)	96.80(0.67)
	L4	80.97	95.57(0.57)	96.14(0.48)	95.04(0.56)	94.45(0.33)	91.76(1.03)	93.12(0.89)	91.89(0.72)	**96.95(0.52)**
	L5	83.90	96.50(0.51)	97.18(0.52)	96.59(0.67)	96.25(0.37)	92.85(1.18)	95.37(0.93)	93.47(0.63)	**98.21(0.35)**
20	L6	84.08	95.11(0.50)	96.17(0.50)	94.45(0.56)	94.11(0.39)	91.49(1.48)	92.16(1.01)	91.33(0.80)	**96.64(0.49)**
	L7	82.48	95.90(0.44)	96.60(0.49)	95.33(0.72)	94.92(0.35)	91.82(1.52)	93.99(0.88)	92.11(0.53)	**97.78(0.43)**
	L8	86.30	96.46(0.44)	97.16(0.39)	96.46(0.32)	95.96(0.37)	92.65(0.99)	94.88(1.03)	93.29(0.88)	**98.12(0.41)**
	L9	85.68	95.98(0.43)	96.85(0.49)	95.37(0.47)	94.91(0.35)	91.58(1.42)	93.81(0.94)	92.05(0.63)	**97.41(0.56)**
	L10	81.55	95.84(0.52)	96.64(0.45)	95.53(0.44)	95.09(0.43)	92.68(1.19)	93.48(0.95)	92.21(0.63)	**97.46(0.43)**
	L11	85.45	96.38(0.41)	97.13(0.43)	96.42(0.37)	96.05(0.38)	92.90(0.99)	95.05(0.94)	93.04(0.55)	**98.12(0.40)**
	L12	83.99	95.13(0.46)	95.85(0.51)	94.87(0.49)	94.53(0.35)	91.90(1.19)	92.40(1.01)	91.55(0.70)	**96.83(0.56)**
Average		83.18	95.91(0.48)	96.68(0.46)	95.59(0.50)	95.12(0.37)	92.09(1.28)	93.88(0.95)	92.29(0.67)	**97.52(0.49)**
p-value		1.22E-04	1.22E-04	2.44E-04	1.22E-04	1.22E-04	1.22E-04	1.22E-04	1.22E-04	–
	L0	80.63	93.69(0.47)	94.60(0.44)	93.14(0.49)	92.42(0.38)	88.78(1.41)	91.05(1.07)	88.90(0.59)	**96.00(0.68)**
	L1	77.97	92.22(0.57)	92.69(0.53)	91.76(0.83)	90.72(0.49)	87.29(0.97)	89.72(0.97)	87.50(0.89)	**94.78(0.86)**
	L2	79.99	93.92(0.45)	94.75(0.41)	93.88(0.64)	93.08(0.35)	89.60(1.09)	91.81(1.07)	89.62(0.75)	**96.03(0.63)**
	L3	78.41	92.75(0.49)	94.11(0.62)	91.62(0.68)	90.66(0.44)	87.18(1.15)	89.52(1.43)	86.98(0.55)	**94.37(0.62)**
	L4	78.27	92.57(0.54)	93.10(0.59)	91.96(0.62)	91.14(0.32)	88.74(1.21)	89.37(1.01)	87.88(0.46)	**93.95(0.54)**
	L5	79.87	93.76(0.52)	94.59(0.43)	94.16(0.52)	93.11(0.39)	90.34(1.27)	92.40(1.09)	89.77(0.74)	**96.14(0.72)**
25	L6	77.69	92.12(0.59)	93.11(0.55)	91.23(0.44)	90.70(0.41)	87.56(1.20)	87.95(1.16)	86.77(0.73)	**93.42(0.59)**
	L7	80.83	93.09(0.54)	93.84(0.44)	92.60(0.49)	91.65(0.40)	88.33(1.18)	90.51(1.09)	88.21(0.66)	**95.39(0.89)**
	L8	80.97	93.83(0.51)	94.65(0.44)	93.64(0.48)	92.70(0.29)	89.60(1.05)	91.87(0.98)	89.30(0.74)	**96.10(0.65)**
	L9	76.59	93.26(0.56)	94.44(0.46)	92.60(0.66)	91.63(0.40)	87.58(1.80)	90.28(1.00)	87.86(0.63)	**95.08(0.68)**
	L10	81.49	93.13(0.57)	93.77(0.46)	92.55(0.85)	91.67(0.38)	88.68(1.17)	90.25(1.03)	88.45(0.68)	**94.87(0.57)**
	L11	78.97	93.81(0.49)	94.48(0.46)	93.77(0.76)	92.91(0.36)	89.67(1.10)	92.20(1.22)	89.55(0.84)	**95.96(0.68)**
	L12	79.59	91.84(0.63)	92.54(0.48)	91.60(0.39)	90.95(0.39)	87.92(1.38)	88.16(1.16)	87.49(0.70)	**93.60(0.50)**
Average		79.33	93.08(0.53)	93.90(0.48)	92.66(0.60)	91.79(0.38)	88.56(1.23)	90.39(1.10)	88.33(0.69)	**95.05(0.66)**
p-value		1.22E-04	1.22E-04	1.22E-04	1.22E-04	1.22E-04	1.22E-04	1.22E-04	1.22E-04	–

Table 4. Performance comparison results of all algorithms under wind scenario 4.

Turbine		NLP	AGA	SUGGA	SHADE	CJADE	CMAES	LSHADE	LSHADE-SPACMA	LSHADE-SPAGA
	L0	86.77	95.25(0.31)	95.38(0.37)	95.76(0.48)	95.94(0.37)	92.54(1.23)	94.52(0.63)	93.60(0.39)	**96.93(0.41)**
	L1	85.98	95.01(0.42)	95.17(0.46)	94.74(0.51)	94.87(0.45)	92.18(1.24)	93.32(0.65)	92.51(0.49)	**95.87(0.64)**
	L2	87.91	95.35(0.38)	95.36(0.31)	95.73(0.40)	96.02(0.29)	93.01(1.17)	94.71(0.66)	93.65(0.44)	**96.79(0.36)**
	L3	84.44	95.10(0.49)	95.18(0.40)	94.65(0.47)	94.96(0.43)	91.98(1.16)	93.29(0.76)	92.30(0.45)	**95.99(0.54)**
	L4	89.40	95.33(0.29)	95.41(0.30)	95.59(0.33)	95.81(0.28)	93.81(0.68)	94.44(0.60)	93.61(0.53)	**96.79(0.30)**
	L5	84.96	95.30(0.31)	95.35(0.33)	95.57(0.43)	95.90(0.29)	94.14(0.98)	94.56(0.66)	93.77(0.45)	**96.62(0.35)**
15	L6	82.24	95.13(0.46)	95.22(0.35)	94.93(0.46)	95.28(0.39)	92.56(1.22)	93.74(0.94)	92.74(0.61)	**96.56(0.39)**
	L7	86.00	95.34(0.36)	95.57(0.41)	95.14(0.51)	95.37(0.39)	92.90(1.10)	93.96(0.72)	93.07(0.60)	**96.40(0.45)**
	L8	86.70	95.28(0.39)	95.30(0.37)	95.63(0.45)	95.98(0.35)	93.45(0.98)	94.78(0.68)	93.65(0.56)	**96.83(0.43)**
	L9	85.15	95.29(0.38)	95.36(0.37)	95.31(0.52)	95.46(0.37)	92.66(1.23)	94.05(0.69)	93.06(0.47)	**96.53(0.65)**
	L10	84.96	95.32(0.35)	95.29(0.30)	95.53(0.47)	95.73(0.29)	93.39(1.08)	94.52(0.62)	93.50(0.41)	**96.83(0.38)**
	L11	89.39	95.35(0.28)	95.27(0.24)	95.60(0.34)	95.84(0.29)	93.63(0.96)	94.53(0.58)	93.60(0.46)	**96.82(0.31)**
	L12	80.25	95.36(0.34)	95.54(0.35)	95.43(0.44)	95.48(0.37)	92.93(1.35)	94.07(0.75)	93.27(0.58)	**96.84(0.49)**
Average		85.70	95.26(0.37)	95.34(0.35)	95.36(0.45)	95.59(0.35)	93.01(1.11)	94.19(0.69)	93.26(0.49)	**96.60(0.44)**
p-value		1.22E-04	1.22E-04	1.22E-04	1.22E-04	1.22E-04	1.22E-04	1.22E-04	1.22E-04	–
	L0	79.35	91.95(0.39)	92.03(0.41)	92.64(0.41)	92.86(0.40)	88.81(1.52)	90.60(0.78)	89.47(0.54)	**93.80(0.53)**
	L1	76.70	91.37(0.48)	91.61(0.58)	90.92(0.42)	91.33(0.36)	88.28(1.05)	88.96(0.77)	87.80(0.48)	**92.17(0.55)**
	L2	82.88	92.01(0.37)	91.99(0.42)	92.55(0.48)	92.90(0.33)	90.06(1.06)	90.67(0.77)	89.56(0.63)	**93.58(0.46)**
	L3	76.26	91.34(0.63)	91.67(0.46)	91.00(0.42)	91.32(0.36)	87.69(1.38)	89.00(0.85)	87.77(0.54)	**92.30(0.57)**
	L4	81.55	91.99(0.32)	92.08(0.48)	92.50(0.38)	92.65(0.33)	90.24(0.67)	90.66(0.79)	89.36(0.52)	**93.73(0.48)**
	L5	83.19	91.94(0.32)	92.06(0.31)	92.60(0.52)	92.87(0.28)	90.68(0.94)	90.59(0.70)	89.68(0.45)	**93.78(0.36)**
20	L6	80.93	91.40(0.50)	91.82(0.42)	91.41(0.47)	91.65(0.44)	88.55(1.15)	89.15(0.91)	88.07(0.56)	**92.96(0.51)**
	L7	78.07	91.83(0.45)	92.03(0.37)	91.83(0.43)	92.15(0.35)	89.06(0.89)	89.97(0.81)	88.67(0.63)	**93.18(0.62)**
	L8	84.16	92.00(0.35)	92.00(0.35)	92.55(0.46)	92.83(0.28)	90.04(1.08)	90.74(0.78)	89.51(0.49)	**93.89(0.63)**
	L9	80.05	91.71(0.50)	92.00(0.44)	91.70(0.48)	92.17(0.39)	88.81(1.17)	89.94(0.79)	88.67(0.43)	**93.18(0.49)**
	L10	82.46	92.03(0.45)	92.01(0.36)	92.49(0.50)	92.73(0.27)	90.17(0.78)	90.41(0.78)	89.46(0.48)	**93.75(0.47)**
	L11	83.61	92.00(0.33)	91.98(0.33)	92.57(0.42)	92.87(0.37)	90.22(0.84)	90.63(0.60)	89.52(0.43)	**93.79(0.39)**
	L12	80.39	91.90(0.37)	92.17(0.33)	92.14(0.54)	92.17(0.28)	89.19(1.04)	89.90(0.87)	88.83(0.68)	**93.45(0.54)**
Average		80.74	91.81(0.42)	91.96(0.40)	92.07(0.46)	92.35(0.34)	89.37(1.04)	90.09(0.78)	88.95(0.53)	**93.35(0.51)**
p-value		1.22E-04	1.22E-04	1.22E-04	1.22E-04	1.22E-04	1.22E-04	1.22E-04	1.22E-04	–
	L0	79.53	88.70(0.33)	88.72(0.29)	89.51(0.39)	89.56(0.42)	86.07(0.98)	86.84(0.75)	85.65(0.53)	**90.65(0.57)**
	L1	75.73	87.89(0.46)	88.03(0.51)	87.42(0.47)	87.67(0.36)	84.62(0.96)	84.93(0.79)	83.59(0.52)	**88.55(0.42)**
	L2	77.85	88.65(0.34)	88.73(0.31)	89.55(0.35)	89.60(0.33)	86.32(1.04)	86.61(0.68)	85.49(0.47)	**90.35(0.43)**
	L3	75.95	87.84(0.57)	88.17(0.52)	87.56(0.40)	87.63(0.32)	84.71(0.84)	84.56(0.66)	83.44(0.42)	**88.66(0.45)**
	L4	80.21	88.81(0.32)	88.82(0.33)	89.33(0.38)	89.47(0.30)	87.02(0.82)	86.53(0.65)	85.60(0.47)	**90.37(0.42)**
	L5	80.72	88.78(0.31)	88.78(0.25)	89.64(0.36)	89.83(0.33)	87.44(0.71)	87.04(0.80)	85.83(0.40)	**90.70(0.38)**
25	L6	78.67	87.77(0.59)	88.10(0.46)	87.89(0.47)	87.98(0.47)	84.55(1.04)	84.91(1.02)	83.66(0.63)	**89.35(0.89)**
	L7	76.54	88.51(0.40)	88.74(0.44)	88.53(0.45)	88.69(0.42)	85.40(0.96)	85.84(0.72)	84.66(0.53)	**89.73(0.48)**
	L8	79.30	88.76(0.39)	88.70(0.34)	89.56(0.36)	89.54(0.30)	85.99(0.94)	86.93(0.78)	85.73(0.62)	**90.57(0.42)**
	L9	73.95	88.31(0.36)	88.52(0.42)	88.57(0.48)	88.70(0.27)	85.57(0.90)	85.74(0.74)	84.54(0.50)	**89.72(0.48)**
	L10	80.59	88.66(0.36)	88.83(0.33)	89.29(0.38)	89.52(0.35)	86.86(0.86)	86.77(0.74)	85.69(0.50)	**90.58(0.47)**
	L11	82.02	88.72(0.32)	88.80(0.32)	89.42(0.43)	89.69(0.29)	87.07(0.79)	87.06(0.85)	85.66(0.41)	**90.59(0.43)**
	L12	77.72	88.44(0.33)	88.74(0.35)	88.68(0.44)	88.91(0.36)	85.71(1.08)	85.86(0.83)	84.69(0.61)	**90.26(0.64)**
Average		78.37	88.45(0.39)	88.59(0.37)	88.84(0.41)	88.99(0.35)	85.95(0.92)	86.12(0.77)	84.94(0.51)	**90.01(0.50)**
p-value		1.22E-04	1.22E-04	1.22E-04	1.22E-04	1.22E-04	1.22E-04	1.22E-04	1.22E-04	–

Figures 7–10 provide box-whisker plots to illustrate the performance variability of various optimization algorithms under specific wind scenarios. Each figure includes three box-whisker plots for turbine counts of 15, 20, and 25, comparing the conversion efficiency of all evaluated algorithms. The box-whisker plot, a statistical tool, depicts the data distribution through a five-number summary: minimum, first quartile, median, third quartile, and maximum. The interquartile range is shown by the box, while the whiskers illustrate the data's spread, and outliers are marked with red plus signs. These plots reveal that the median conversion efficiency tends to decline with an increase in turbine number.

The diversity in the spread and range across the algorithms may indicate their varying stability and performance consistency. The figures demonstrate that LSHADE-SPACMA consistently delivers stable and high-quality solutions for WFLO problems.

Figures 11–14 depict the optimal wind farm layouts derived from all tested algorithms. Each figure contains a set of grid layouts, each illustrating the solution provided by a different algorithm for scenarios involving either 20 or 25 turbines. Below each grid, the algorithm's name is displayed, accompanied by the conversion efficiency (η) achieved by the layout it generated. The grids are sequentially numbered to denote possible turbine locations, with uniquely colored stars or symbols marking the actual turbine placements. All tested algorithms are distinguished by distinct symbols and colors, facilitating a straightforward visual comparison of their respective solutions. Notably, LSHADE-SPAGA consistently generates the best wind farm layouts, adhering to the constraints and effectively mitigating wake effects.

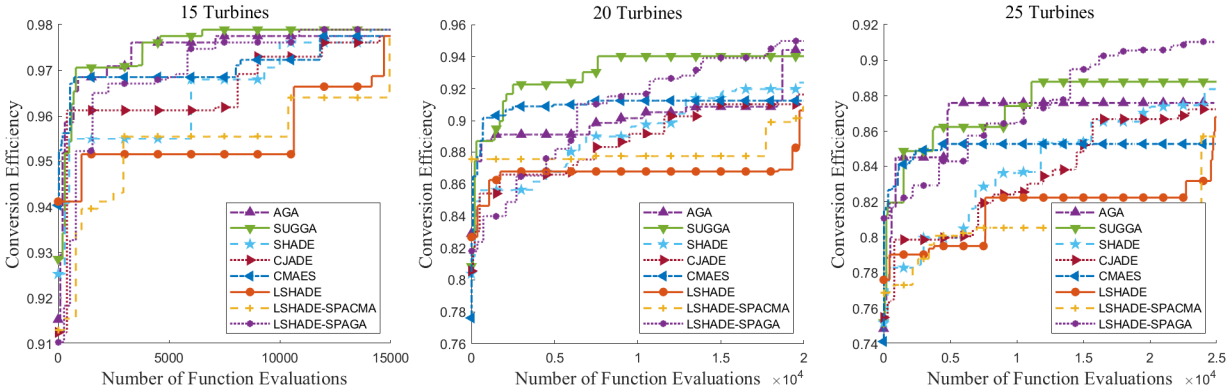

Figure 3. The convergence plots of all compared algorithms for wind scenario 1.

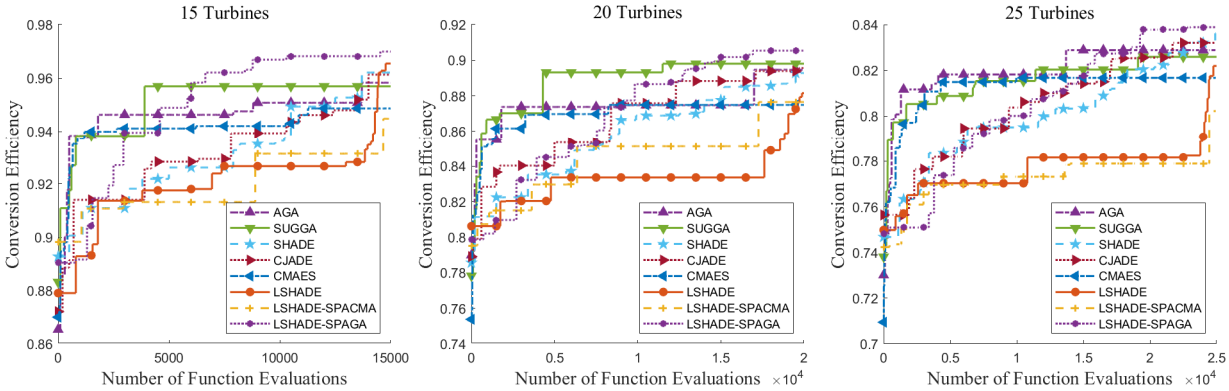

Figure 4. The convergence plots of all compared algorithms for wind scenario 2.

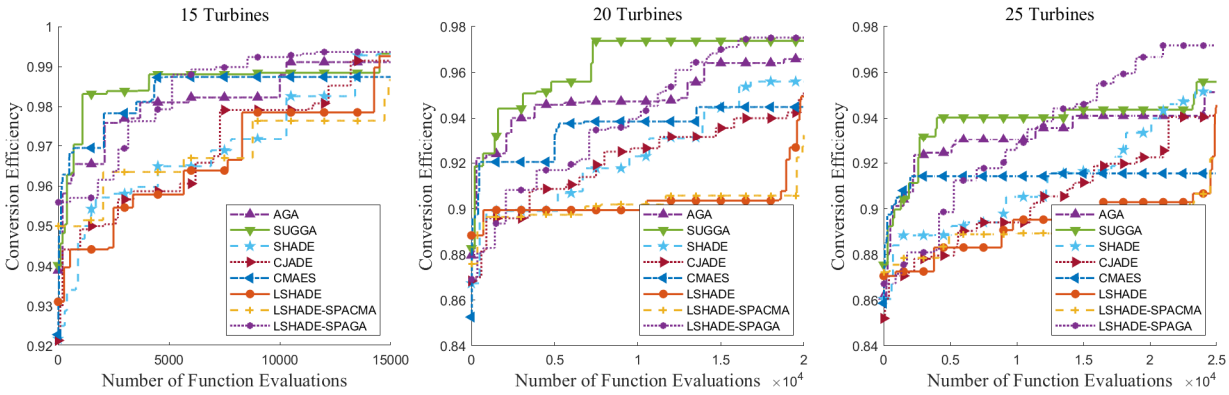

Figure 5. The convergence plots of all compared algorithms for wind scenario 3.

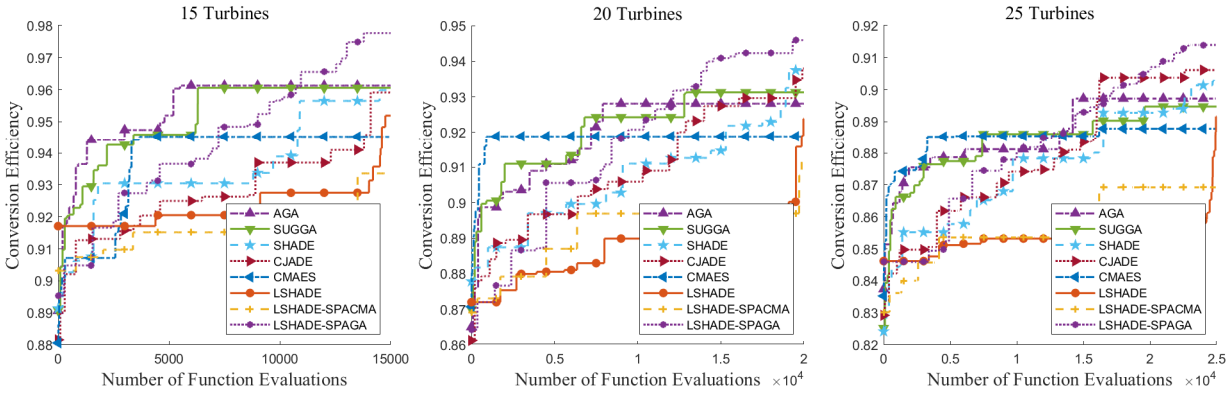

Figure 6. The convergence plots of all compared algorithms for wind scenario 4.

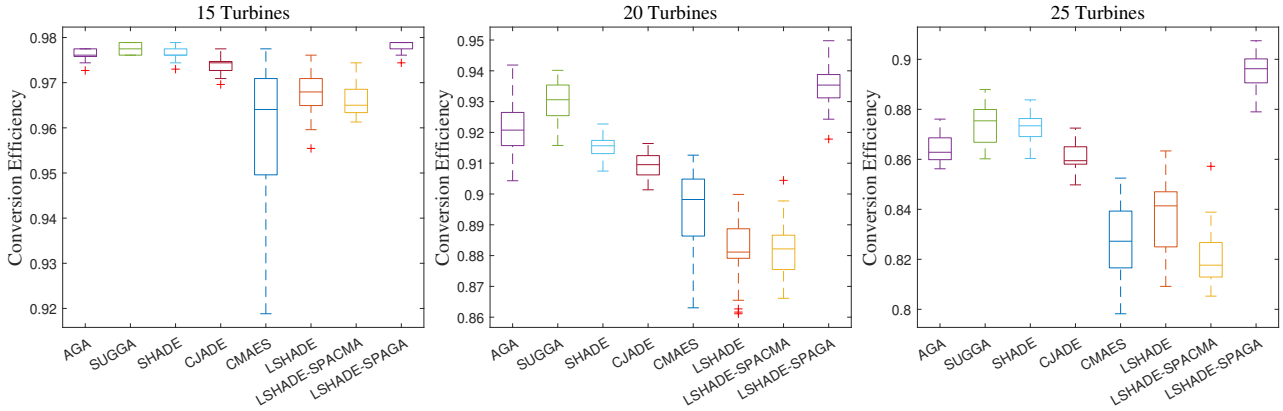

Figure 7. The box-whisker plots for wind scenario 1.

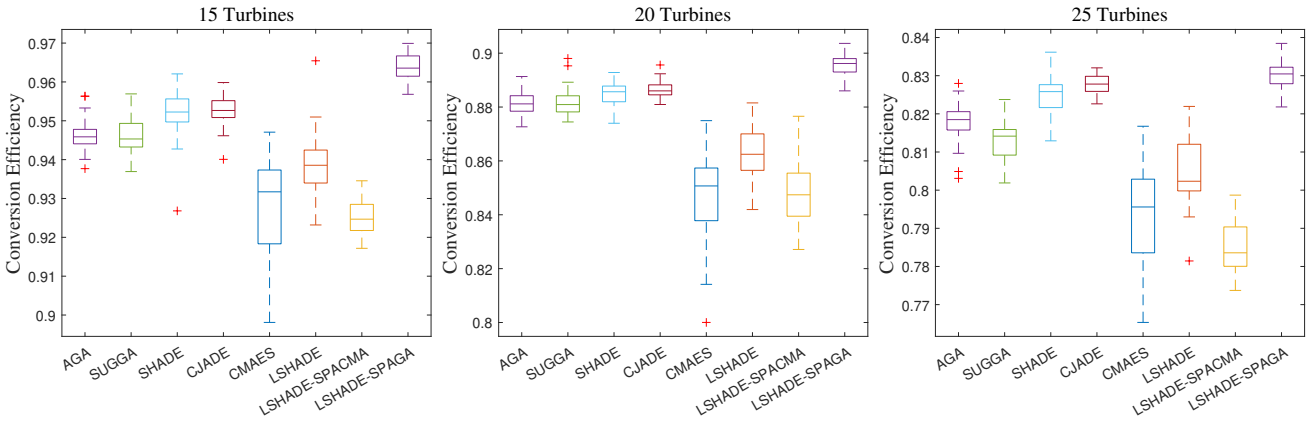

Figure 8. The box-whisker plots for wind scenario 2.

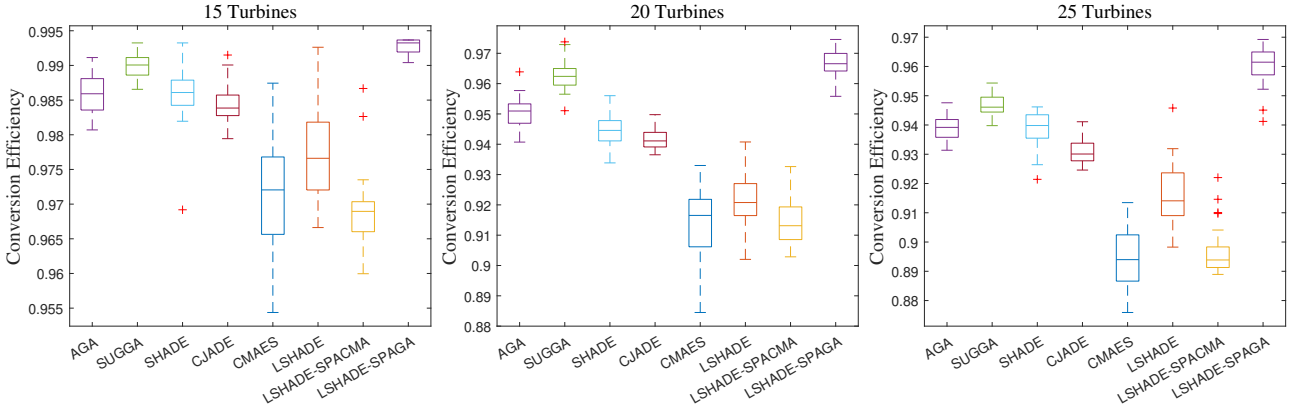

Figure 9. The box-whisker plots for wind scenario 3.

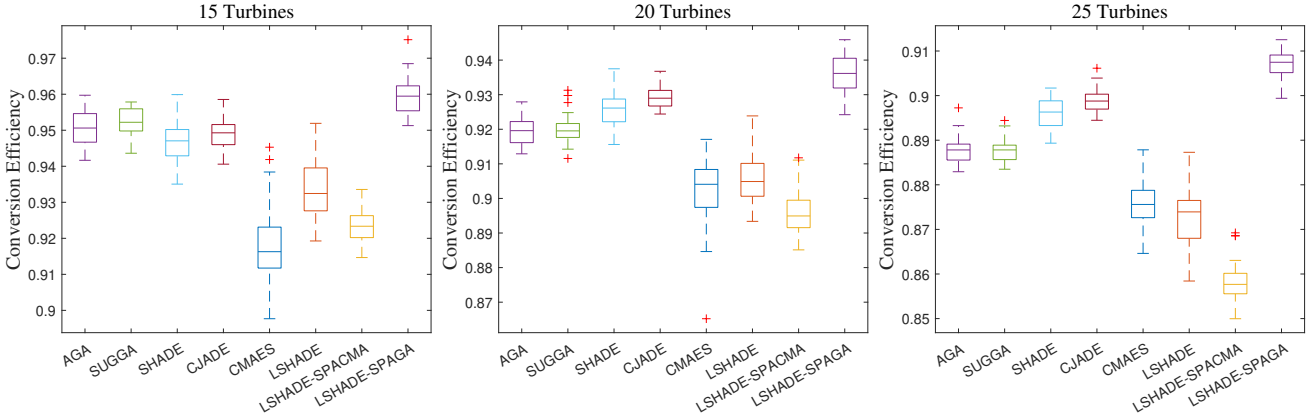

Figure 10. The box-whisker plots for wind scenario 4.

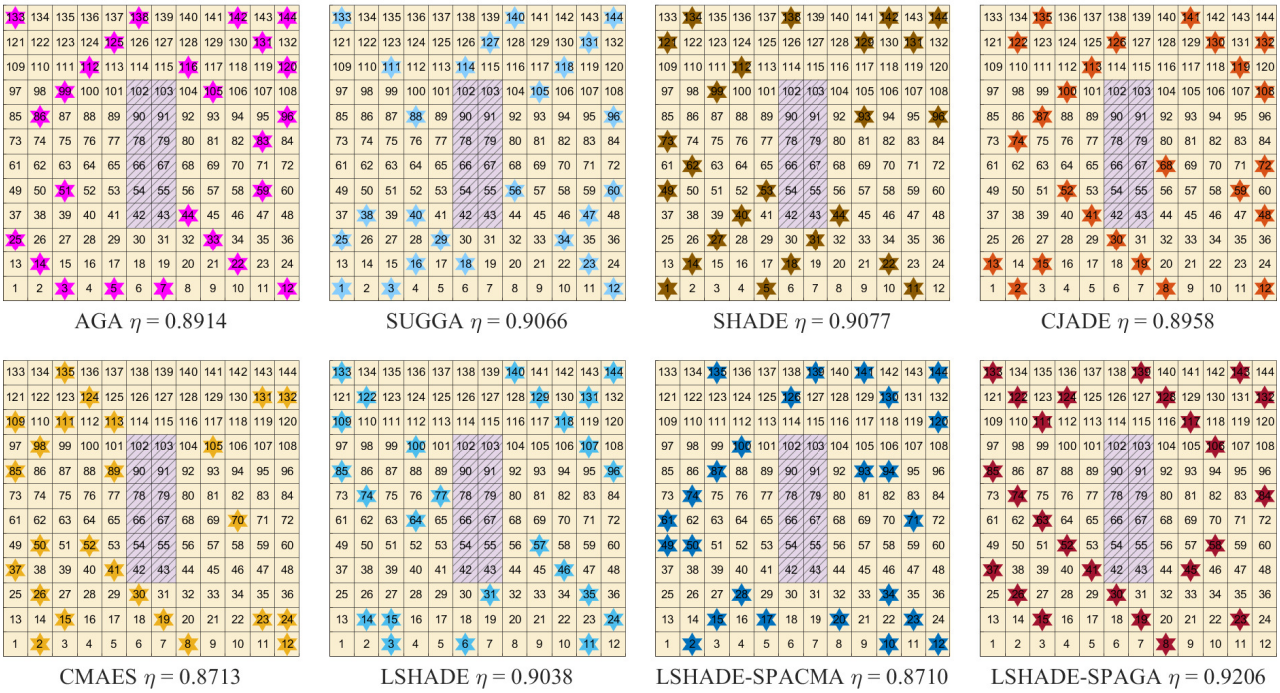

Figure 11. The wind farm layout obtained by all compared algorithms for wind scenario 1 with 25 turbines.

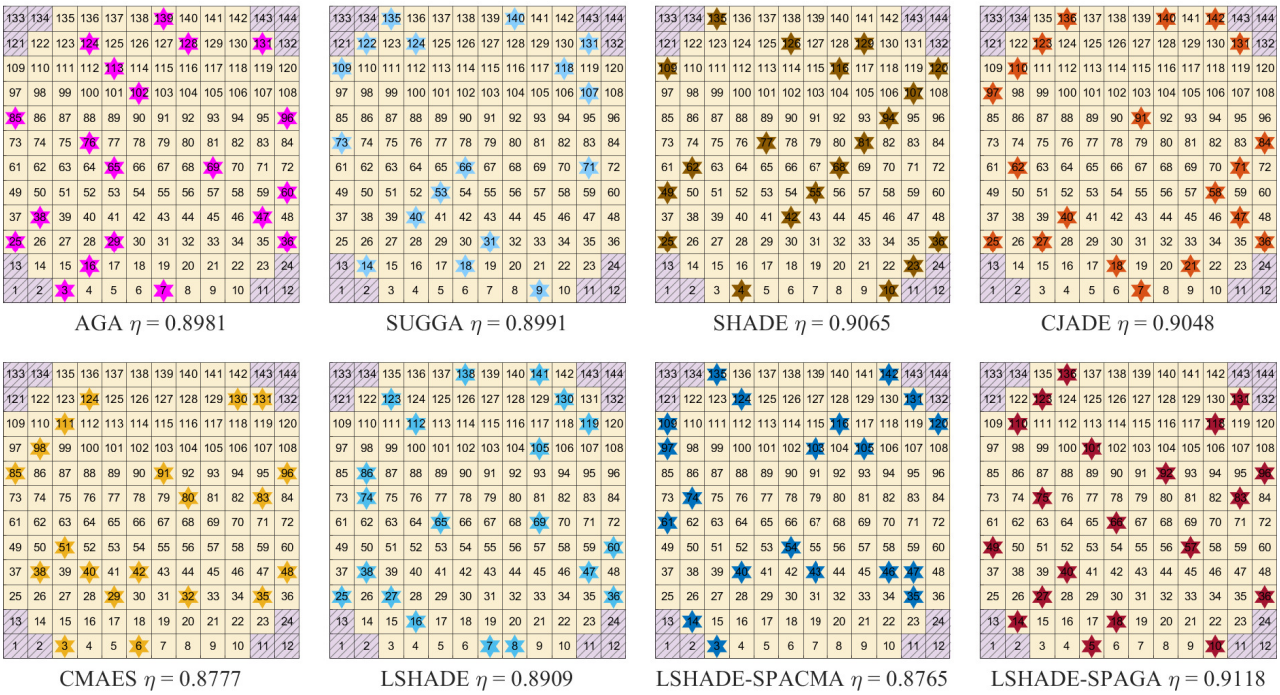

Figure 12. The wind farm layout obtained by all compared algorithms for wind scenario 2 with 20 turbines.

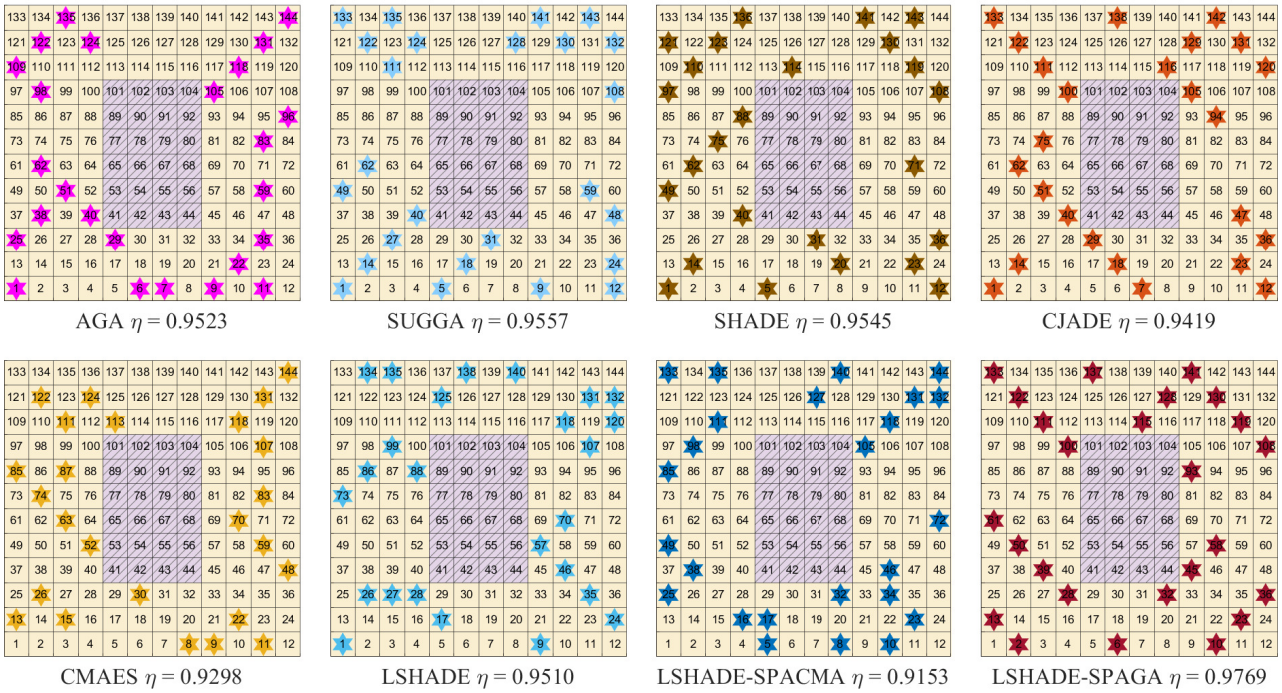

Figure 13. The wind farm layout obtained by all compared algorithms for wind scenario 3 with 25 turbines.

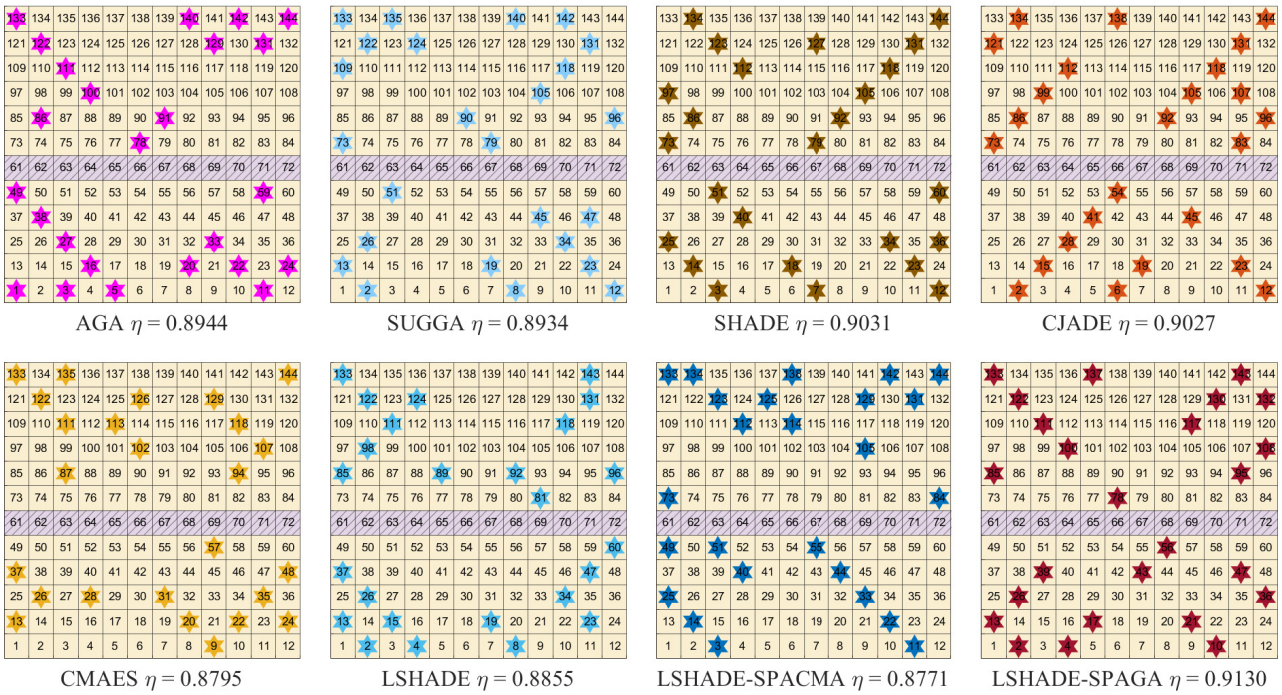

Figure 14. The wind farm layout obtained by all compared algorithms for wind scenario 4 with 25 turbines.

4.3. Ablation study and discussions

In this section, we perform an ablation study regarding the mutation and crossover operators used in the proposed LSHADE-SPAGA. Table 5 summarizes four combinations of different strategies, where the Mutation-CMA denotes the ones used in CMA-ES, the Mutation-GA means the genetic mutation operator defined in Eq (3.2). Crossover-DE represents the original operator in DE. Crossover-GA denotes the crossover operator defined in Eq (3.3). Table 6 presents a detailed comparison of the effects of varying mutation and crossover strategies on the performance of LSHADE-SPAGA across four different wind scenarios (WS1, WS2, WS3, and WS4). Each wind scenario section is divided into rows representing different constraints (L1 to L12) and columns representing the strategies (S1, S2, S3, and S4). The performance under each constraint and strategy is quantified by a numerical value, with the standard deviation in parentheses. The table evaluates the effectiveness of these strategies in optimizing the conversion efficiency within wind farm layouts. From it, it is clear that the combination of the proposed Eqs (3.2) and (3.3) yields the best performance. Additionally, those p-values at the bottom of each wind scenario section statistically evaluates the significance of the results, which suggests that the proposed genetic operators significantly enhance the search performance of the algorithm.

In this section, we conduct an ablation study to examine the impact of different mutation and crossover operators on the proposed LSHADE-SPAGA algorithm. Table 5 details four distinct strategy combinations, with "Mutation-CMA" referring to operators used in CMA-ES, and "Mutation-GA" indicating the genetic mutation operator as defined in Eq (3.2). "Crossover-DE" pertains to the original operator in DE, while "Crossover-GA" refers to the crossover operator outlined in Eq (3.3). Table 6 provides a comprehensive comparison of these strategies' impact on LSHADE-SPAGA's performance across four separate wind scenarios (WS1-WS4). These scenarios are categorized by various constraints (L_1 to $L12$) and strategies (S1-S4), with the algorithm's effectiveness under each scenario being measured by numerical values accompanied by their standard deviations. It becomes evident that integrating the proposed Eqs (3.2) and (3.3) results in superior performance. Furthermore, the p-values included at the end of each section statistically affirm the significance of the results, indicating that the customized genetic operators substantially improve the algorithm's search capabilities.

This study delves into the hyper-parameter N_{min}. As indicated by Eq (3.4), a minimum of four individuals is required to execute a DE mutation. We have set N_{min} to 4, D, and $2D$ for analysis. Generally, a greater N_{min} could potentially bolster the local exploitation ability of an algorithm, albeit possibly at the expense of computational efficiency. Table 7 investigates the influence of the minimum population size on the algorithm's performance over four wind scenarios (WS1-WS4), considering different turbine counts (15, 20, and 25).

Additionally, Table 8 presents the results of the Wilcoxon rank-sum test, applied to discuss the hyper-parameter. The findings from these tables suggest that, while a larger N_{min} may yield better solutions for WFLO in some cases, marked improvements are not consistently observed. Consequently, to balance solution quality with computational efficiency, we opt for the minimum permissible value of N_{min}, which is 4, in this research.

Table 5. The combination of different strategies.

Strategies	Crossover-DE	Crossover-GA
Mutation-CMA	S1	S2
Mutation-GA	S3	S4

Table 6. The ablation results of four different combinations of mutation and crossover operators.

Parameter		S1	S2	S3	S4	S1	S2	S3	S4	S1	S2	S3	S4
Turbine		15				20				25			
	L0	96.59(0.50)	97.64(0.19)	97.50(0.28)	**97.82(0.12)**	90.14(0.79)	93.81(0.73)	92.44(0.68)	**94.93(0.43)**	83.53(0.97)	88.33(1.25)	85.83(0.85)	**90.63(0.67)**
	L1	95.60(0.52)	96.76(0.19)	96.56(0.30)	**96.91(0.11)**	88.31(0.99)	92.08(0.80)	90.42(0.74)	**93.24(0.35)**	80.69(0.97)	85.96(1.26)	82.80(1.12)	**88.13(0.81)**
	L2	97.03(0.39)	97.76(0.12)	97.64(0.27)	**97.85(0.07)**	91.79(0.98)	94.44(0.52)	94.01(0.57)	**95.08(0.30)**	84.76(0.83)	88.78(1.25)	87.96(0.98)	**91.00(0.61)**
	L3	93.82(0.61)	95.68(0.53)	95.36(0.34)	**96.16(0.22)**	85.97(0.86)	90.31(1.38)	88.79(1.19)	**92.54(0.85)**	77.59(0.73)	82.09(1.12)	80.13(1.27)	**84.14(0.50)**
	L4	93.85(0.76)	95.63(0.39)	95.10(0.58)	**96.11(0.27)**	85.88(1.08)	89.88(1.29)	89.07(0.76)	**92.64(0.73)**	77.78(1.02)	81.75(1.01)	80.48(0.77)	**84.09(0.51)**
	L5	97.00(0.39)	97.82(0.10)	97.69(0.24)	**97.87(0.06)**	91.80(1.06)	94.72(0.51)	93.97(0.97)	**95.28(0.30)**	84.58(1.09)	89.54(1.17)	87.61(1.36)	**91.33(0.54)**
WS1	L6	95.92(0.68)	97.35(0.30)	97.27(0.32)	**97.78(0.14)**	88.26(0.99)	90.88(1.00)	90.59(0.71)	**93.55(0.67)**	79.86(0.72)	83.61(0.92)	82.75(0.87)	**87.22(0.54)**
	L7	96.05(0.49)	97.24(0.20)	97.08(0.34)	**97.42(0.10)**	89.10(1.01)	92.94(0.73)	91.49(0.65)	**94.03(0.42)**	81.88(1.09)	87.12(1.38)	84.49(0.86)	**89.56(0.68)**
	L8	96.84(0.32)	97.75(0.15)	97.70(0.20)	**97.84(0.09)**	91.08(0.93)	94.14(0.67)	93.20(0.76)	**95.01(0.30)**	84.24(0.97)	88.87(1.09)	87.10(0.69)	**90.85(0.60)**
	L9	95.35(0.65)	96.76(0.31)	96.37(0.49)	**97.00(0.15)**	88.15(0.79)	92.16(1.05)	90.91(0.55)	**94.11(0.58)**	80.88(0.84)	85.18(1.23)	83.44(1.00)	**87.54(0.57)**
	L10	95.31(0.54)	96.77(0.30)	96.46(0.32)	**96.99(0.15)**	88.38(1.01)	92.18(0.93)	90.80(0.93)	**93.91(0.54)**	80.82(0.81)	85.27(1.19)	83.14(1.01)	**87.41(0.52)**
	L11	96.79(0.41)	97.72(0.16)	97.68(0.13)	**97.86(0.07)**	90.68(0.96)	94.29(0.68)	93.40(0.64)	**95.09(0.38)**	83.90(1.00)	89.36(1.13)	86.46(1.36)	**91.01(0.63)**
	L12	96.13(0.61)	97.35(0.30)	97.25(0.39)	**97.76(0.14)**	89.02(0.96)	92.58(0.90)	91.47(0.88)	**94.13(0.53)**	81.61(0.99)	86.07(1.24)	84.41(0.75)	**89.00(0.76)**
p-value		1.22E-04	1.22E-04	1.22E-04	–	1.22E-04	1.22E-04	1.22E-04	–	1.22E-04	1.22E-04	1.22E-04	–
	L0	90.14(0.79)	93.81(0.73)	92.44(0.68)	**94.93(0.43)**	83.53(0.97)	88.33(1.25)	85.83(0.85)	**90.63(0.67)**	93.88(0.73)	96.28(0.42)	95.71(0.64)	**96.97(0.35)**
	L1	88.31(0.99)	92.08(0.80)	90.42(0.74)	**93.24(0.35)**	80.69(0.97)	85.96(1.26)	82.80(1.12)	**88.13(0.81)**	91.54(0.73)	93.94(0.52)	93.49(0.61)	**94.69(0.35)**
	L2	91.79(0.98)	94.44(0.52)	94.01(0.57)	**95.08(0.30)**	84.76(0.83)	88.78(1.25)	87.96(0.98)	**91.00(0.61)**	92.29(0.70)	94.72(0.47)	94.59(0.46)	**95.40(0.31)**
	L3	85.97(0.86)	90.31(1.38)	88.79(1.19)	**92.54(0.85)**	77.59(0.73)	82.09(1.12)	80.13(1.27)	**84.14(0.50)**	91.26(0.84)	93.87(0.58)	93.65(0.64)	**94.71(0.37)**
	L4	85.88(1.08)	89.88(1.29)	89.07(0.76)	**92.64(0.73)**	77.78(1.02)	81.75(1.01)	80.48(0.77)	**84.09(0.51)**	92.08(0.68)	94.19(0.50)	94.35(0.65)	**95.33(0.29)**
	L5	91.80(1.06)	94.72(0.51)	93.97(0.97)	**95.28(0.30)**	84.58(1.09)	89.54(1.17)	87.61(1.36)	**91.33(0.54)**	92.59(0.60)	95.65(0.56)	95.06(0.80)	**96.38(0.34)**
WS2	L6	88.26(0.99)	90.88(1.00)	90.59(0.71)	**93.55(0.67)**	79.86(0.72)	83.61(0.92)	82.75(0.87)	**87.22(0.54)**	92.88(0.88)	95.60(0.63)	95.36(0.77)	**96.51(0.29)**
	L7	89.10(1.01)	92.94(0.73)	91.49(0.65)	**94.03(0.42)**	81.88(1.09)	87.12(1.38)	84.49(0.86)	**89.56(0.68)**	92.93(0.76)	95.28(0.48)	94.80(0.52)	**95.82(0.35)**
	L8	91.08(0.93)	94.14(0.67)	93.20(0.76)	**95.01(0.30)**	84.24(0.97)	88.87(1.09)	87.10(0.69)	**90.85(0.60)**	93.21(0.70)	95.56(0.49)	95.24(0.59)	**96.23(0.41)**
	L9	88.15(0.79)	92.16(1.05)	90.91(0.55)	**94.11(0.58)**	80.88(0.84)	85.18(1.23)	83.44(1.00)	**87.54(0.57)**	92.50(0.68)	95.20(0.54)	94.78(0.66)	**95.91(0.41)**
	L10	88.38(1.01)	92.18(0.93)	90.80(0.93)	**93.91(0.54)**	80.82(0.81)	85.27(1.19)	83.14(1.01)	**87.41(0.52)**	92.91(0.73)	95.39(0.60)	95.10(0.62)	**96.14(0.37)**
	L11	90.68(0.96)	94.29(0.68)	93.40(0.64)	**95.09(0.38)**	83.90(1.00)	89.36(1.13)	86.46(1.36)	**91.01(0.63)**	93.48(0.85)	96.06(0.51)	95.58(0.64)	**96.70(0.32)**
	L12	89.02(0.96)	92.58(0.90)	91.47(0.88)	**94.13(0.53)**	81.61(0.99)	86.07(1.24)	84.41(0.75)	**89.00(0.76)**	93.48(0.68)	96.04(0.51)	95.68(0.65)	**96.54(0.30)**
p-value		1.22E-04	1.22E-04	1.22E-04	–	1.22E-04	1.22E-04	1.22E-04	–	1.22E-04	1.22E-04	1.22E-04	–
	L0	83.53(0.97)	88.33(1.25)	85.83(0.85)	**90.63(0.67)**	93.88(0.73)	96.28(0.42)	95.71(0.64)	**96.97(0.35)**	86.73(0.88)	89.86(0.62)	88.75(0.70)	**90.90(0.45)**
	L1	80.69(0.97)	85.96(1.26)	82.80(1.12)	**88.13(0.81)**	91.54(0.73)	93.94(0.52)	93.49(0.61)	**94.69(0.35)**	83.32(0.93)	86.12(0.63)	85.06(0.54)	**87.06(0.50)**
	L2	84.76(0.83)	88.78(1.25)	87.96(0.98)	**91.00(0.61)**	92.29(0.70)	94.72(0.47)	94.59(0.46)	**95.40(0.31)**	84.76(0.73)	87.88(0.71)	87.34(0.77)	**89.00(0.39)**
	L3	77.59(0.73)	82.09(1.12)	80.13(1.27)	**84.14(0.50)**	91.26(0.84)	93.87(0.58)	93.65(0.64)	**94.71(0.37)**	82.95(0.90)	85.92(0.74)	84.97(0.85)	**87.24(0.40)**
	L4	77.78(1.02)	81.75(1.01)	80.48(0.77)	**84.09(0.51)**	92.08(0.68)	94.19(0.50)	94.35(0.65)	**95.33(0.29)**	84.45(0.72)	87.30(0.78)	87.04(0.85)	**88.89(0.38)**
	L5	84.58(1.09)	89.54(1.17)	87.61(1.36)	**91.33(0.54)**	92.59(0.60)	95.65(0.56)	95.06(0.80)	**96.38(0.34)**	85.22(0.69)	88.44(0.64)	87.96(0.71)	**89.68(0.41)**
WS3	L6	79.86(0.72)	83.61(0.92)	82.75(0.87)	**87.22(0.54)**	92.88(0.88)	95.60(0.63)	95.36(0.77)	**96.51(0.29)**	84.84(1.03)	87.79(0.80)	87.24(0.69)	**89.61(0.40)**
	L7	81.88(1.09)	87.12(1.38)	84.49(0.86)	**89.56(0.68)**	92.93(0.76)	95.28(0.48)	94.80(0.52)	**95.82(0.35)**	85.18(0.95)	88.19(0.64)	87.12(0.68)	**89.26(0.39)**
	L8	84.24(0.97)	88.87(1.09)	87.10(0.69)	**90.85(0.60)**	93.21(0.70)	95.56(0.49)	95.24(0.59)	**96.23(0.41)**	85.76(0.87)	88.96(0.72)	87.91(0.86)	**90.12(0.48)**
	L9	80.88(0.84)	85.18(1.23)	83.44(1.00)	**87.54(0.57)**	92.50(0.68)	95.20(0.54)	94.78(0.66)	**95.91(0.41)**	84.85(0.67)	87.87(0.67)	86.82(0.77)	**89.22(0.41)**
	L10	80.82(0.81)	85.27(1.19)	83.14(1.01)	**87.41(0.52)**	92.91(0.73)	95.39(0.60)	95.10(0.62)	**96.14(0.37)**	85.44(0.73)	88.69(0.82)	87.99(0.85)	**90.07(0.41)**
	L11	83.90(1.00)	89.36(1.13)	86.46(1.36)	**91.01(0.63)**	93.48(0.85)	96.06(0.51)	95.58(0.64)	**96.70(0.32)**	86.21(0.75)	89.32(0.72)	88.42(0.80)	**90.46(0.39)**
	L12	81.61(0.99)	86.07(1.24)	84.41(0.75)	**89.00(0.76)**	93.48(0.68)	96.04(0.51)	95.68(0.65)	**96.54(0.30)**	85.89(0.78)	88.90(0.69)	87.94(0.77)	**90.39(0.44)**
p-value		1.22E-04	1.22E-04	1.22E-04	–	1.22E-04	1.22E-04	1.22E-04	–	1.22E-04	1.22E-04	1.22E-04	–
	L0	93.88(0.73)	96.28(0.42)	95.71(0.64)	**96.97(0.35)**	86.73(0.88)	89.86(0.62)	88.75(0.70)	**90.90(0.45)**	79.86(0.79)	83.01(0.59)	81.59(0.45)	**84.25(0.40)**
	L1	91.54(0.73)	93.94(0.52)	93.49(0.61)	**94.69(0.35)**	83.32(0.93)	86.12(0.63)	85.06(0.54)	**87.06(0.50)**	75.40(0.67)	78.49(0.61)	77.12(0.43)	**79.45(0.36)**
	L2	92.29(0.70)	94.72(0.47)	94.59(0.46)	**95.40(0.31)**	84.76(0.73)	87.88(0.71)	87.34(0.77)	**89.00(0.39)**	77.33(0.75)	80.43(0.68)	79.33(0.78)	**81.98(0.39)**
	L3	91.26(0.84)	93.87(0.58)	93.65(0.64)	**94.71(0.37)**	82.95(0.90)	85.92(0.74)	84.97(0.85)	**87.24(0.40)**	74.97(0.55)	78.06(0.57)	76.56(0.75)	**79.50(0.40)**
	L4	92.08(0.68)	94.19(0.50)	94.35(0.65)	**95.33(0.29)**	84.45(0.72)	87.30(0.78)	87.04(0.85)	**88.89(0.38)**	77.20(0.86)	80.15(0.80)	79.28(0.81)	**82.05(0.33)**
	L5	92.59(0.60)	95.65(0.56)	95.06(0.80)	**96.38(0.34)**	85.22(0.69)	88.44(0.64)	87.96(0.71)	**89.68(0.41)**	78.35(0.63)	81.91(0.63)	80.65(0.81)	**83.39(0.32)**
WS4	L6	92.88(0.88)	95.60(0.63)	95.36(0.77)	**96.51(0.29)**	84.84(1.03)	87.79(0.80)	87.24(0.69)	**89.61(0.40)**	77.04(0.70)	80.36(0.97)	79.19(0.78)	**82.78(0.37)**
	L7	92.93(0.76)	95.28(0.48)	94.80(0.52)	**95.82(0.35)**	85.18(0.95)	88.19(0.64)	87.12(0.68)	**89.26(0.39)**	77.79(0.57)	81.01(0.67)	79.66(0.52)	**82.05(0.41)**
	L8	93.21(0.70)	95.56(0.49)	95.24(0.59)	**96.23(0.41)**	85.76(0.87)	88.96(0.72)	87.91(0.86)	**90.12(0.48)**	78.49(0.67)	81.89(0.66)	80.44(0.70)	**83.07(0.40)**
	L9	92.50(0.68)	95.20(0.54)	94.78(0.66)	**95.91(0.41)**	84.85(0.67)	87.87(0.67)	86.82(0.77)	**89.22(0.41)**	77.48(0.69)	80.62(0.54)	79.26(0.76)	**82.06(0.41)**
	L10	92.91(0.73)	95.39(0.60)	95.10(0.62)	**96.14(0.37)**	85.44(0.73)	88.69(0.82)	87.99(0.85)	**90.07(0.41)**	78.54(0.76)	81.67(0.83)	80.20(0.57)	**83.20(0.43)**
	L11	93.48(0.85)	96.06(0.51)	95.58(0.64)	**96.70(0.32)**	86.21(0.75)	89.32(0.72)	88.42(0.80)	**90.46(0.39)**	79.25(0.76)	82.59(0.82)	81.13(0.79)	**83.99(0.35)**
	L12	93.48(0.68)	96.04(0.51)	95.68(0.65)	**96.54(0.30)**	85.89(0.78)	88.90(0.69)	87.94(0.77)	**90.39(0.44)**	78.61(0.74)	82.10(0.69)	80.12(0.69)	**83.76(0.39)**
p-value		1.22E-04	1.22E-04	1.22E-04	–	1.22E-04	1.22E-04	1.22E-04	–	1.22E-04	1.22E-04	1.22E-04	–

Table 7. The discussion of minimum population size on the performance of the proposed algorithm.

Parameter		4.0	D	2D	4.0	D	2D	4.0	D	2D
Turbine		15			20			25		
	L0	**97.80(0.10)**	97.81(0.09)	97.80(0.10)	94.93(0.43)	**94.75(0.46)**	94.75(0.46)	**90.55(0.69)**	90.62(0.75)	90.55(0.69)
	L1	**96.90(0.12)**	96.88(0.10)	96.90(0.12)	**92.99(0.56)**	93.08(0.46)	92.99(0.56)	**87.90(0.80)**	88.02(0.80)	87.90(0.80)
	L2	**97.84(0.08)**	97.85(0.07)	97.84(0.08)	95.08(0.30)	**95.11(0.39)**	95.11(0.39)	**90.99(0.52)**	90.99(0.49)	90.99(0.52)
	L3	**96.16(0.23)**	96.11(0.29)	96.16(0.23)	92.54(0.85)	**92.67(0.65)**	92.67(0.65)	84.14(0.50)	84.27(0.51)	**84.28(0.47)**
	L4	96.11(0.27)	**96.12(0.26)**	96.12(0.26)	92.64(0.73)	**92.72(0.78)**	92.72(0.78)	84.09(0.51)	**84.14(0.46)**	84.14(0.46)
	L5	97.87(0.06)	97.88(0.05)	**97.88(0.04)**	95.28(0.30)	95.24(0.31)	**95.28(0.30)**	91.33(0.54)	91.35(0.45)	**91.42(0.57)**
WS1	L6	**97.72(0.14)**	97.77(0.11)	97.72(0.14)	93.55(0.67)	93.68(0.62)	**93.80(0.67)**	**87.15(0.60)**	87.04(0.69)	87.15(0.60)
	L7	**97.38(0.13)**	97.38(0.13)	97.38(0.13)	94.03(0.42)	**93.93(0.51)**	93.93(0.51)	**89.45(0.68)**	89.56(0.55)	89.45(0.68)
	L8	**97.80(0.10)**	97.84(0.09)	97.80(0.10)	95.01(0.30)	**94.97(0.38)**	94.97(0.38)	90.85(0.60)	**90.84(0.58)**	90.84(0.58)
	L9	97.00(0.15)	**96.96(0.20)**	96.96(0.20)	**93.97(0.63)**	94.05(0.49)	93.97(0.63)	87.54(0.57)	**87.52(0.58)**	87.52(0.58)
	L10	96.99(0.15)	97.00(0.17)	**97.00(0.17)**	**93.74(0.63)**	93.84(0.60)	93.74(0.63)	87.41(0.52)	**87.50(0.54)**	87.50(0.54)
	L11	**97.85(0.06)**	97.84(0.08)	97.85(0.06)	**95.06(0.37)**	95.06(0.42)	95.06(0.37)	91.01(0.63)	90.97(0.50)	**91.01(0.75)**
	L12	**97.69(0.18)**	97.73(0.16)	97.69(0.18)	94.13(0.53)	**94.12(0.56)**	94.12(0.56)	89.00(0.76)	**89.07(0.70)**	89.07(0.70)
	L0	94.93(0.43)	**94.75(0.46)**	94.75(0.46)	**90.55(0.69)**	90.62(0.75)	90.55(0.69)	**96.81(0.31)**	96.86(0.32)	96.81(0.31)
	L1	**92.99(0.56)**	93.08(0.46)	92.99(0.56)	**87.90(0.80)**	88.02(0.80)	87.90(0.80)	94.69(0.35)	**94.55(0.41)**	94.55(0.41)
	L2	95.08(0.30)	**95.11(0.39)**	95.11(0.39)	**90.99(0.52)**	90.99(0.49)	90.99(0.52)	**95.36(0.39)**	95.38(0.27)	95.36(0.39)
	L3	92.54(0.85)	**92.67(0.65)**	92.67(0.65)	84.14(0.50)	84.27(0.51)	**84.28(0.47)**	94.71(0.37)	**94.62(0.42)**	94.62(0.42)
	L4	92.64(0.73)	**92.72(0.78)**	92.72(0.78)	84.09(0.51)	**84.14(0.46)**	84.14(0.46)	**95.19(0.40)**	95.25(0.37)	95.19(0.40)
	L5	95.28(0.30)	95.24(0.31)	**95.28(0.30)**	91.33(0.54)	91.35(0.45)	**91.42(0.57)**	**96.36(0.40)**	96.33(0.36)	96.36(0.40)
WS2	L6	93.55(0.67)	93.68(0.62)	**93.80(0.67)**	**87.15(0.60)**	87.04(0.69)	87.15(0.60)	**96.36(0.30)**	96.43(0.33)	96.36(0.30)
	L7	94.03(0.42)	**93.93(0.51)**	93.93(0.51)	**89.45(0.68)**	89.56(0.55)	89.45(0.68)	95.82(0.35)	**95.85(0.38)**	95.85(0.38)
	L8	95.01(0.30)	**94.97(0.38)**	94.97(0.38)	90.85(0.60)	**90.84(0.58)**	90.84(0.58)	**96.19(0.33)**	96.23(0.33)	96.19(0.33)
	L9	**93.97(0.63)**	94.05(0.49)	93.97(0.63)	87.54(0.57)	**87.52(0.58)**	87.52(0.58)	**95.90(0.38)**	95.86(0.41)	95.90(0.38)
	L10	**93.74(0.63)**	93.84(0.60)	93.74(0.63)	87.41(0.52)	**87.50(0.54)**	87.50(0.54)	**96.12(0.34)**	96.09(0.32)	96.12(0.34)
	L11	**95.06(0.37)**	95.06(0.42)	95.06(0.37)	91.01(0.63)	90.97(0.50)	**91.01(0.75)**	96.70(0.32)	**96.65(0.40)**	96.65(0.40)
	L12	94.13(0.53)	**94.12(0.56)**	94.12(0.56)	89.00(0.76)	**89.07(0.70)**	89.07(0.70)	96.54(0.30)	96.51(0.32)	**96.64(0.31)**
	L0	**90.55(0.69)**	90.62(0.75)	90.55(0.69)	**96.81(0.31)**	96.86(0.32)	96.81(0.31)	**90.85(0.46)**	90.81(0.42)	90.85(0.46)
	L1	**87.90(0.80)**	88.02(0.80)	87.90(0.80)	94.69(0.35)	**94.55(0.41)**	94.55(0.41)	87.06(0.50)	87.15(0.36)	**87.16(0.36)**
	L2	**90.99(0.52)**	90.99(0.49)	90.99(0.52)	**95.36(0.39)**	95.38(0.27)	95.36(0.39)	89.00(0.39)	89.03(0.46)	**89.10(0.36)**
	L3	84.14(0.50)	84.27(0.51)	**84.28(0.47)**	94.71(0.37)	**94.62(0.42)**	94.62(0.42)	**87.22(0.43)**	87.15(0.41)	87.22(0.43)
	L4	84.09(0.51)	**84.14(0.46)**	84.14(0.46)	**95.19(0.40)**	95.25(0.37)	95.19(0.40)	88.89(0.38)	89.04(0.41)	**89.07(0.44)**
	L5	91.33(0.54)	91.35(0.45)	**91.42(0.57)**	**96.36(0.40)**	96.33(0.36)	96.36(0.40)	**89.64(0.30)**	89.65(0.34)	89.64(0.30)
WS3	L6	**87.15(0.60)**	87.04(0.69)	87.15(0.60)	**96.36(0.30)**	96.43(0.33)	96.36(0.30)	89.61(0.40)	89.55(0.50)	**89.63(0.39)**
	L7	**89.45(0.68)**	89.56(0.55)	89.45(0.68)	95.82(0.35)	**95.85(0.38)**	95.85(0.38)	89.26(0.39)	89.15(0.47)	**89.41(0.41)**
	L8	90.85(0.60)	**90.84(0.58)**	90.84(0.58)	**96.19(0.33)**	96.23(0.33)	96.19(0.33)	**90.05(0.46)**	90.04(0.45)	90.05(0.46)
	L9	87.54(0.57)	**87.52(0.58)**	87.52(0.58)	**95.90(0.38)**	95.86(0.41)	95.90(0.38)	89.22(0.41)	**89.30(0.41)**	89.30(0.41)
	L10	87.41(0.52)	**87.50(0.54)**	87.50(0.54)	**96.12(0.34)**	96.09(0.32)	96.12(0.34)	90.07(0.41)	90.01(0.43)	**90.10(0.36)**
	L11	91.01(0.63)	90.97(0.50)	**91.01(0.75)**	96.70(0.32)	**96.65(0.40)**	96.65(0.40)	90.46(0.39)	**90.40(0.37)**	90.40(0.37)
	L12	89.00(0.76)	**89.07(0.70)**	89.07(0.70)	96.54(0.30)	96.51(0.32)	**96.64(0.31)**	90.39(0.44)	90.42(0.48)	**90.46(0.53)**
	L0	**96.81(0.31)**	96.86(0.32)	96.81(0.31)	**90.85(0.46)**	90.81(0.42)	90.85(0.46)	84.25(0.40)	84.21(0.38)	**84.32(0.43)**
	L1	94.69(0.35)	**94.55(0.41)**	94.55(0.41)	87.06(0.50)	87.15(0.36)	**87.16(0.36)**	79.45(0.36)	79.53(0.38)	**79.57(0.38)**
	L2	**95.36(0.39)**	95.38(0.27)	95.36(0.39)	89.00(0.39)	89.03(0.46)	**89.10(0.36)**	**81.95(0.39)**	81.95(0.43)	81.95(0.39)
	L3	94.71(0.37)	**94.62(0.42)**	94.62(0.42)	**87.22(0.43)**	87.15(0.41)	87.22(0.43)	79.50(0.40)	79.49(0.40)	**79.65(0.37)**
	L4	**95.19(0.40)**	95.25(0.37)	95.19(0.40)	88.89(0.38)	89.04(0.41)	**89.07(0.44)**	82.05(0.33)	82.04(0.37)	**82.10(0.37)**
	L5	**96.36(0.40)**	96.33(0.36)	96.36(0.40)	**89.64(0.30)**	89.65(0.34)	89.64(0.30)	**83.36(0.41)**	83.36(0.35)	83.36(0.41)
WS4	L6	**96.36(0.30)**	96.43(0.33)	96.36(0.30)	89.61(0.40)	89.55(0.50)	**89.63(0.39)**	**82.74(0.41)**	82.72(0.42)	82.74(0.41)
	L7	95.82(0.35)	**95.85(0.38)**	95.85(0.38)	89.26(0.39)	89.15(0.47)	**89.41(0.41)**	82.05(0.41)	**82.11(0.36)**	82.11(0.36)
	L8	**96.19(0.33)**	96.23(0.33)	96.19(0.33)	**90.05(0.46)**	90.04(0.45)	90.05(0.46)	83.07(0.40)	83.10(0.43)	**83.35(0.40)**
	L9	**95.90(0.38)**	95.86(0.41)	95.90(0.38)	89.22(0.41)	**89.30(0.41)**	89.30(0.41)	**82.05(0.42)**	82.01(0.38)	82.05(0.42)
	L10	**96.12(0.34)**	96.09(0.32)	96.12(0.34)	90.07(0.41)	90.01(0.43)	**90.10(0.36)**	83.20(0.43)	83.29(0.37)	**83.37(0.37)**
	L11	96.70(0.32)	**96.65(0.40)**	96.65(0.40)	90.46(0.39)	**90.40(0.37)**	90.40(0.37)	83.99(0.35)	**84.03(0.37)**	84.03(0.37)
	L12	96.54(0.30)	96.51(0.32)	**96.64(0.31)**	90.39(0.44)	90.42(0.48)	**90.46(0.53)**	83.76(0.39)	83.70(0.42)	**83.81(0.37)**

Table 8. Wilcoxon rank-sum test results of the minimum population size on the performance of the proposed algorithm.

Turbine	15	20	25	15	20	25	15	20	25	15	20	25
Wind scenarios	WS1			WS2			WS3			WS4		
D	0/13/0	1/11/1	0/13/0	1/12/0	0/13/0	1/12/0	1/11/1	0/13/0	1/10/2	2/10/1	0/13/0	0/12/1
2D	2/11/0	2/10/1	0/12/1	4/9/0	0/12/1	0/10/3	1/11/1	0/13/0	0/12/1	3/10/0	1/11/1	2/11/0

5. Conclusions

In this paper, we propose LSHADE-SPAGA, a cutting-edge algorithm that enhances the differential evolution process with a binary genetic operator for optimizing environmental concerns, particularly focusing on wind farm layout optimization (WFLO). This innovation comes in response to the urgent need for sustainable resource management amid escalating environmental challenges and rapid economic growth. The LSHADE-SPAGA algorithm underwent rigorous testing across various conditions, including four distinct wind scenarios, twelve specific layout constraints, an unconstrained layout option, and three different turbine types, resulting in a comprehensive evaluation over 156 test cases. It was compared with seven leading algorithms, and the results demonstrated that LSHADE-SPAGA consistently delivered superior solution quality and achieved a well-balanced trade-off between the speed of convergence and the accuracy of results. Its capacity to navigate effectively between global exploration and local exploitation proves crucial in addressing the intricacies of WFLO. The algorithm's marked ability to escape local optima and produce high-quality solutions marks a significant contribution to the field of environmental optimization for wind farm layouts. Looking ahead, there are plans to extend the application of LSHADE-SPAGA to a broader range of complex environmental optimization challenges.

Use of AI tools declaration

The authors declare they have not used Artificial Intelligence (AI) tools in the creation of this article.

Acknowledgments

This reserch was partially supported by the Science and Technology Plan Project of Changzhou (CJ20210155, CJ20220174), Natural Science Foundation of the Jiangsu Higher Education Institutions of China (23KJA520001, 21KJD520002), Jiangsu Province Vocational College Teacher Professional Leader High-end Training Project under Grant (2023TDFX003) and Qing-Lan Project of Jiangsu Province.

Conflict of interest

The authors declare there is no conflict of interest.

References

1. Abido MA (2003) Environmental/economic power dispatch using multiobjective evolutionary algorithms. *IEEE Trans Power Syst* 18: 1529–1537. https://doi.org/10.1109/TPWRS.2003.818693
2. Lei ZY, Gao SC, Zhang ZM, et al. (2023) A chaotic local search-based particle swarm optimizer for large-scale complex wind farm layout optimization. *IEEE/CAA J Autom Sin* 10: 1168–1180. https://doi.org/10.1109/JAS.2023.123387
3. Lei ZY, Gao SC, Wang YR, et al. (2022) An adaptive replacement strategy-incorporated particle swarm optimizer for wind farm layout optimization. *Energy Convers Manage* 269: 116174. https://doi.org/10.1016/j.enconman.2022.116174
4. Lei ZY, Gao SC, Zhang ZM, et al. (2022) MO4: A many-objective evolutionary algorithm for protein structure prediction. *IEEE Trans Evol Comput* 26: 417–430. https://doi.org/10.1109/TEVC.2021.3095481
5. Wang YR, Yu Y, Cao SY, et al. (2020) A review of applications of artificial intelligent algorithms in wind farms. *Artif Intell Rev* 53: 3447–3500. https://doi.org/10.1007/s10462-019-09768-7
6. Kiehbadroudinezhad M, Merabet M, Rajabipour A, et al. (2020) Optimization of wind/solar energy microgrid by division algorithm considering human health and environmental impacts for power-water cogeneration. *Energy Convers Manage* 252: 115064. https://doi.org/10.1016/j.enconman.2021.115064
7. Reddy SR (2020) Wind farm layout optimization (WindFLO): An advanced framework for fast wind farm analysis and optimization. *Appl Energy* 269: 115090. https://doi.org/10.1016/j.apenergy.2020.115090
8. Liu ZQ, Peng J, Hua X, et al. (2021) Wind farm optimization considering non-uniformly distributed turbulence intensity. *Sustainable Energy Technol Assess* 43: 100970. https://doi.org/10.1016/j.seta.2020.100970
9. Gualtieri G (2020) Comparative analysis and improvement of grid-based wind farm layout optimization. *Energy Convers Manage* 208: 112593. https://doi.org/10.1016/j.enconman.2020.112593
10. Moreno SR, Pierezan J, dos Santos Coelho L, et al. (2021) Multi-objective lightning search algorithm applied to wind farm layout optimization. *Energy* 216: 119214. https://doi.org/10.1016/j.energy.2020.119214
11. Beşkirli M, Koç İ, Haklı H, et al. (2018) A new optimization algorithm for solving wind turbine placement problem: Binary artificial algae algorithm. *Renewable Energy* 121: 301–308. https://doi.org/10.1016/j.renene.2017.12.087
12. Nash R, Nouri R, Vasel-Be-Hagh A (2021) Wind turbine wake control strategies: A review and concept proposal. *Energy Convers Manage* 245: 114581. https://doi.org/10.1016/j.enconman.2021.114581
13. Lee CY, Hasegawa H, Gao SC (2022) Complex-valued neural networks: A comprehensive survey. *IEEE/CAA J Autom Sin* 9: 1406–1426. https://doi.org/10.1109/JAS.2022.105743

14. Wang RL, Lei ZZ, Zhang ZM, et al. (2022) Dendritic convolutional neural network. *IEEJ Trans Electr Electron Eng* 17: 302–304. https://doi.org/10.1002/tee.23513
15. Yu Y, Lei ZZ, Wang YR, et al. (2022) Improving dendritic neuron model with dynamic scale-free network-based differential evolution. *IEEE/CAA J Autom Sin* 9: 99–110. https://doi.org/10.1109/JAS.2021.1004284
16. Garcia Marquez FP, Peinado Gonzalo A (2022) A comprehensive review of artificial intelligence and wind energy. *Arch Comput Methods Eng* 29: 2935–2958. https://doi.org/10.1007/s11831-021-09678-4
17. Lei ZY, Gao SC, Hasegawa H, et al. (2023) Fully complex-valued gated recurrent neural network for ultrasound imaging. *IEEE Trans Neural Networks Learn Syst*, 1–14. https://doi.org/10.1109/TNNLS.2023.3282231
18. Yu XB, Lu YC (2023) Reinforcement learning-based multi-objective differential evolution for wind farm layout optimization. *Energy* 284: 129300. https://doi.org/10.1016/j.energy.2023.129300
19. Bai FY, Ju XL, Wang SY, et al. (2022) Wind farm layout optimization using adaptive evolutionary algorithm with monte carlo tree search reinforcement learning. *Energy Convers Manage* 252: 115047. https://doi.org/10.1016/j.enconman.2021.115047
20. Asaah P, Hao LL, Ji J (2021) Optimal placement of wind turbines in wind farm layout using particle swarm optimization. *J Mod Power Syst Clean Energy* 9: 367–375. https://doi.org/10.35833/MPCE.2019.000087
21. Reddy SR (2021) An efficient method for modeling terrain and complex terrain boundaries in constrained wind farm layout optimization. *Renewable Energy* 165: 162–173. https://doi.org/10.1016/j.renene.2020.10.076
22. Mittal P, Mitra K (2020) In search of flexible and robust wind farm layouts considering wind state uncertainty. *J Cleaner Prod* 248: 119195. https://doi.org/10.1016/j.jclepro.2019.119195
23. Chen K, Song MX, Zhang X, et al. (2016) Wind turbine layout optimization with multiple hub height wind turbines using greedy algorithm. *Renewable Energy* 96: 676–686. https://doi.org/10.1016/j.renene.2016.05.018
24. Guirguis D, Romero DA, Amon CH (2016) Toward efficient optimization of wind farm layouts: Utilizing exact gradient information. *Appl Energy* 179: 110–123. https://doi.org/10.1016/j.apenergy.2016.06.101
25. Rehman S, Khan SA, Alhems LM (2020) A rule-based fuzzy logic methodology for multi-criteria selection of wind turbines. *Sustainability* 12: 8467. https://doi.org/10.3390/su12208467
26. Grady S, Hussaini M, Abdullah MM (2005) Placement of wind turbines using genetic algorithms. *Renewable Energy* 30: 259–270. https://doi.org/10.1016/j.renene.2004.05.007
27. Zhong L, Sui QY, Yu JTY, et al. (2023) Elite-of-the-elites driven five-layered gravitational search algorithm for optimization. *IEEJ Trans Electr Electron Eng* 18: 1958–1960. https://doi.org/10.1002/tee.23921
28. Sui QY, Zhong L, Yu JTY, et al. (2023) Particle swarm optimization with average individuals distance-incorporated exploitation. *IEEJ Trans Electr Electron Eng* 18: 1722–1724. https://doi.org/10.1002/tee.23896

29. Wang ZQ, Gao SC, Zhou MC, et al. (2023) Information-theory-based nondominated sorting ant colony optimization for multiobjective feature selection in classification. *IEEE Trans Cybern* 53: 5276–5289. https://doi.org/10.1016/j.asoc.2023.110064

30. Wang KY, Wang YR, Tao SC, et al. (2023) Spherical search algorithm with adaptive population control for global continuous optimization problems. *Appl Soft Comput* 132: 109845. https://doi.org/10.1016/j.asoc.2022.109845

31. Yu Y, Gao SC, Zhou MC, et al. (2022) Scale-free network-based differential evolution to solve function optimization and parameter estimation of photovoltaic models. *Swarm Evol Comput* 74: 101142. https://doi.org/10.1016/j.swevo.2022.101142

32. Xu Z, Gao SC, Yang HC, et al. (2021) SCJADE: Yet another state-of-the-art differential evolution algorithm. *IEEJ Trans Electr Electron Eng* 16: 644–646. https://doi.org/10.1002/tee.23340

33. Gao SC, Wang KY, Tao SC, et al. (2021) A state-of-the-art differential evolution algorithm for parameter estimation of solar photovoltaic models. *Energy Convers Manage* 230: 113784. https://doi.org/10.1016/j.enconman.2020.113784

34. Qureshi TA, Warudkar V (2023) Wind farm layout optimization through optimal wind turbine placement using a hybrid particle swarm optimization and genetic algorithm. *Environ Sci Pollut Res* 30: 77436–77452. https://doi.org/10.1007/s11356-023-27849-7

35. Yang HC, Gao SC, Lei ZY, et al. (2023) An improved spherical evolution with enhanced exploration capabilities to address wind farm layout optimization problem. *Eng Appl Artif Intell* 123: 106198. https://doi.org/10.1016/j.engappai.2023.106198

36. Yu Y, Zhang TF, Lei ZZ, et al. (2023) A chaotic local search-based LSHADE with enhanced memory storage mechanism for wind farm layout optimization. *Appl Soft Comput* 141: 110306. https://doi.org/10.1016/j.asoc.2023.110306

37. Kunakote T, Sabangban N, Kumar S, et al. (2022) Comparative performance of twelve metaheuristics for wind farm layout optimisation. *Arch Comput Methods Eng* 29: 717–730. https://doi.org/10.1007/s11831-021-09586-7

38. Long H, Li PK, Gu W (2020) A data-driven evolutionary algorithm for wind farm layout optimization. *Energy* 208: 118310. https://doi.org/10.1016/j.energy.2020.118310

39. Gao SC, Zhou MC, Wang YR, et al. (2019) Dendritic neuron model with effective learning algorithms for classification, approximation, and prediction. *IEEE Trans Neural Networks Learn Syst* 30: 601–604. https://doi.org/10.1109/TNNLS.2018.2846646

40. Gao SC, Zhou MC, Wang ZQ, et al. (2023) Fully complex-valued dendritic neuron model. *IEEE Trans Neural Networks Learn Syst* 34: 2105–2118. https://doi.org/10.1109/TNNLS.2021.3105901

41. Ju X, Liu F (2019) Wind farm layout optimization using self-informed genetic algorithm with information guided exploitation. *Appl Energy* 248: 429–445. https://doi.org/10.1016/j.apenergy.2019.04.084

42. Ju XL, Liu F, Wang L, et al. (2019) Wind farm layout optimization based on support vector regression guided genetic algorithm with consideration of participation among landowners. *Energy Convers Manage* 196: 1267–1281. https://doi.org/10.1016/j.enconman.2019.06.082

43. Zhang YY, Chen GY, Cheng L, et al. (2019) Methods to balance the exploration and exploitation in differential evolution from different scales: A survey. *Neurocomputing* 561: 126899. https://doi.org/10.1016/j.neucom.2023.126899

44. Zhang ZH, Yu QR, Yang HC, et al. (2024) Triple-layered chaotic differential evolution algorithm for layout optimization of offshore wave energy converters. *Expert Syst Appl* 239: 122439. https://doi.org/10.1016/j.eswa.2023.122439

45. Cai ZH, Yang X, Zhou MC, et al. (2023) Toward explicit control between exploration and exploitation in evolutionary algorithms: A case study of differential evolution. *Inf Sci* 649: 119656. https://doi.org/10.1016/j.ins.2023.119656

46. Gupta S, Singh S, Su R, et al. (2023) Multiple elite individual guided piecewise search-based differential evolution. *IEEE/CAA J Autom Sin* 10: 135–158. https://doi.org/10.1109/JAS.2023.123018

47. Li XS, Li JY, Yang HC, et al. (2022) Population interaction network in representative differential evolution algorithms: Power-law outperforms Poisson distribution. *Phys A* 603: 127764. https://doi.org/10.1016/j.physa.2022.127764

48. Yu Y, Wang KY, Zhang TF, et al. (2022) A population diversity-controlled differential evolution for parameter estimation of solar photovoltaic models. *Sustainable Energy Technol Assess* 51: 101938. https://doi.org/10.1016/j.seta.2021.101938

49. Tanabe R, Fukunaga AS (2014) Improving the search performance of SHADE using linear population size reduction. *2014 IEEE Congress on Evolutionary Computation (CEC)*, Beijing, China, 1658–1665. https://doi.org/10.1109/CEC.2014.6900380

50. Mohamed AW, Hadi AA, Fattouh AM, et al. (2022) LSHADE with semi-parameter adaptation hybrid with CMA-ES for solving CEC 2017 benchmark problems. *2017 IEEE Congress on Evolutionary Computation (CEC)*, Donostia, Spain, 145–152. https://doi.org/10.1109/CEC.2017.7969307

51. Mosetti G, Poloni C, Diviacco B (1994) Optimization of wind turbine positioning in large windfarms by means of a genetic algorithm. *J Wind Eng Ind Aerodyn* 51: 105–116. https://doi.org/10.1016/0167-6105(94)90080-9

52. Shakoor R, Hassan MY, Raheem A, et al. (2016) Wake effect modeling: A review of wind farm layout optimization using Jensen's model. *Renewable Sustainable Energy Rev* 58: 1048–1059. https://doi.org/10.1016/j.rser.2015.12.229

53. Rao RV, Keesari HS (2018) Multi-team perturbation guiding jaya algorithm for optimization of wind farm layout. *Appl Soft Comput* 71: 800–815. https://doi.org/10.1016/j.asoc.2018.07.036

54. Sorkhabi SYD, Romero DA, Beck JC, et al. (2018) Constrained multi-objective wind farm layout optimization: Novel constraint handling approach based on constraint programming. *Renewable Energy* 126: 341–353. https://doi.org/10.1016/j.renene.2018.03.053

55. Zergane S, Smaili A, Masson C (2018) Optimization of wind turbine placement in a wind farm using a new pseudo-random number generation method. *Renewable Energy* 125: 166–171. https://doi.org/10.1016/j.renene.2018.02.082

56. Rizk-Allah RM, Hassanien AE (2023) A hybrid equilibrium algorithm and pattern search technique for wind farm layout optimization problem. *ISA Trans* 132: 402–418. https://doi.org/10.1016/j.isatra.2022.06.014

57. Sun HY, Yang HX (2023) Wind farm layout and hub height optimization with a novel wake model. *Appl Energy* 348: 121554. https://doi.org/10.1016/j.apenergy.2023.121554

58. González JS, Rodriguez AGG, Mora JC, et al. (2010) Optimization of wind farm turbines layout using an evolutive algorithm. *Renewable Energy* 35: 1671–1681. https://doi.org/10.1016/j.renene.2010.01.010

59. Abdelsalam AM, El-Shorbagy MA (2018) Optimization of wind turbines siting in a wind farm using genetic algorithm based local search. *Renewable Energy* 123: 748–755. https://doi.org/10.1016/j.renene.2018.02.083

60. Wolpert DH, Macready WG (1997) No free lunch theorems for optimization. *IEEE Trans Evol Comput* 1: 67–82. https://doi.org/10.1109/4235.585893

61. Sui QY, Yu Y, Wang KY, et al. (2024) Best-worst individuals driven multiple-layered differential evolution. *Inf Sci* 655: 119889. https://doi.org/10.1016/j.ins.2023.119889

62. Tanabe R, Fukunaga A (2013) Success-history based parameter adaptation for differential evolution. *2013 IEEE Congress on Evolutionary Computation*, Cancun, Mexico, 71–78. https://doi.org/10.1109/CEC.2013.6557555

63. Gao SC, Yu Y, Wang YR (2021) Chaotic local search-based differential evolution algorithms for optimization. *IEEE Trans Syst Man Cybern: Syst* 51: 3954–3967. https://doi.org/10.1109/TSMC.2019.2956121

64. Hansen N (2006) Advances on estimation of distribution algorithms. In: Jose A. Lozano, Pedro Larrañaga, Iñaki Inza, Endika Bengoetxea, *Towards a New Evolutionary Computation*, 1st Ed, Springer Berlin, Heidelberg. 192: 75–102. https://doi.org/10.1007/3-540-32494-1_4

AIMS Press